Chapter 4

Synthesis and study of donor-acceptor type π-conjugated polymers based on carbazole and isoindigo units

Table of contents

Introduction **134**

Results and discussion **141**

Synthesis of monomers 141

Synthesis of polymers 142

Molecular weight and thermal properties of polymers 143

Photophysical properties of polymers 144

Electrochemical properties of polymers 145

X-ray diffraction studies of polymers 147

Atomic Force Microscopy (AFM) analysis 148

Space Charge Limited Current (SCLC) measurement of polymers 149

Conclusion **153**

Experimental procedures **154**

General procedure 154

Synthesis of 9-dodecyl-3,6-bis(4,4,5,5-tetramethyl-1,3,2-dioxaborolan-2-yl)-9*H*-carbazole 154

Synthesis of monomers 156

Synthesis of (3Z,3'Z)-3,3'-(1,4-phenylenebis(methaneylylidene)) bis(5-bromo-1-tetradecylindolin-2-one) **(M1)** 156

Synthesis of (3Z,3'Z)-3,3'-(thiophene-2,5-diylbis(methaneylylidene)bis(5-bromo-1-tetradecylindolin-2-one) **(M2)** 156

Synthesis of (3Z,3'Z)-3,3'-((2,5-bis(dodecyloxy)-1,4-phenylene) bis (methaneylylidene)) bis(5-bromo-1-tetradecylindolin-2-one) **(M3)** 157

Synthesis of polymers 157

General procedure for synthesis of carbazole based conjugated polymers **TIIG-BP**, **THP-BP** and **DAB-BP** 157

Spectral data 159

References 167

Introduction

In recent years, conjugated carbazole polymers have indeed become a subject of growing interest due to their notable properties such as strong fluorescence and excellent hole transporting abilities.[1] The arrangement of the carbazole units within the polymer chain significantly influences its properties. Poly(3,6-carbazole) represents one of the early classes of conjugated carbazole polymers.[2] In these polymers, the carbazole units are connected either directly or through π-spacers, as depicted in Figure 4.1.[3] This connectivity pattern plays a crucial role in determining the electronic and optical properties of the polymers. Stability of Poly(3,6-carbazole) in both oxidized and excited states, making them suitable candidates for various applications including electrochemical and phosphorescent devices. This stability enhances their performance and extends their potential applications in organic electronic devices.[4–6]

Carbazole-containing polymers indeed hold significant promise across a range of applications in photonics and organic electronics. Their versatile properties, including photophysical characteristics, hole-transporting abilities, photoconductivity, and electroluminescence, make them highly desirable for various technologies such as Lighty Emitting Diodes (LEDs) Organic photovoltaics (OPVs), Organic Field Effect Transistors (OFETs), sensors, electrochromic devices, and more.[7,8] This versatility stems from the unique structure and behaviour of carbazole units when incorporated into the polymer backbone, allowing for tailored performance in specific applications.[9] As research in this field continues to advance, we can expect further innovations and optimizations in the design and synthesis of these polymers, unlocking even more potential for practical applications.[10,11]

The establishment of an efficient synthetic route for 2,7-dihalocarbazole derivatives marked a significant development.[12] This led to the emergence of poly(2,7-carbazole) as an attractive alternative to blue-light fluorescent polyfluorene derivatives.[13] The latter suffered from photodegradation issues, resulting in changes in colour emission and optical instability. Subsequently, researchers discovered that conjugated copolymers combining the electron-donating 2,7-carbazole with electron-accepting π-systems exhibited promising characteristics as p-type semiconductors for bulk heterojunction solar cells. Polymers incorporating carbazole moieties either in the main chain or side chain have garnered significant interest due to their distinctive

properties stemming from carbazole.[14] These properties render them suitable for a wide array of photonic applications, including photoconductive, electroluminescent, and photorefractive materials.[5,14] This discovery sparked renewed interest in developing conjugated carbazole polymers with various connectivities to further enhance their properties.[15] For instance, poly(2,9-carbazole) and poly(3,9-carbazole) have been synthesized recently, and their properties have been thoroughly investigated. These efforts contribute to the expanding repertoire of materials available for applications in optoelectronic devices, particularly in solar cell technology.[13,16,17]

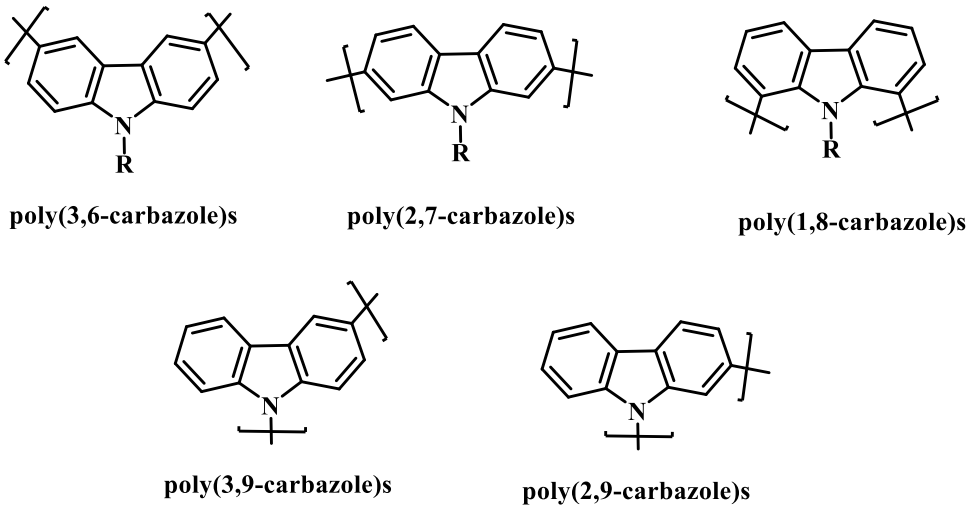

Figure 4.1 Structure of conjugated carbazole with different connectives.

Recent years have seen a significant amount of research on conjugated polymers with carbazole units in the main chain; these characteristics of polymers are influenced by the unit of carbazolene replacement locations. It is easy for derivatives of poly(2,7-carbazole) and poly(3,6-carbazole) to produce homogenous layers. Because of their rod-like shape, derivatives of poly(2,7-carbazole) have a lower bandgap energy. Thus, it is anticipated that poly(2,7-carbazole) will be helpful for materials used in hole transmission.[17–20]

Since their special qualities enable a variety of optoelectronic applications, including photoconductive, electroluminescent, electrochromic, and photorefractive materials, polymers with carbazole moieties in the main chain or side chain have garnered plenty of interest. Because carbazole-based derivatives exhibit both high triplet energy levels and carrier transport capabilities at the same time, they have been employed as efficient host materials for phosphorescent metal complexes *via* the

formation of oligocarbazoles or carbazole dendrons *via* 3(6), 9linkages. Without changing the planar shape of the resultant polymers, carbazole can be replaced or polymerized at the 2 and 7 or 3 and 6 locations.[21] A broad range of alkyl and aryl chains can also be put on the nitrogen atom.[22] The physicchemical characteristics of poly(3,6-carbazole)s and poly(2,7-carbazole)s may be optimised by various synthetic processes and substitution patterns, resulting in high-performing materials for various electronic applications.[14,23,24]

However, Ambrose and Nelson were the first to investigate the electrochemical oxidation of carbazole and N-substituted derivatives.[25] They used spectroscopic and electrochemical methods to conduct a systematic study on the substituent effects of ring-substituted carbazoles.[26] N-Phenylcarbazoles (NPCs) consisting of both unprotected carbazole ring positions (3 and 6).[3,21,27] These compounds were first subjected to one electron oxidation, which produced a highly reactive cation radical.[28–30] Two of these radicals then linked at the 3 locations, resulting in the formation of an N,N'-diphenyl-3,3'-bicarbazyl. Effective use of this carbazole oxidative dimerization process has produced electroactive polymeric films with potential uses in optoelectronic and electronic devices.[31,32] When synthesising conducting polymer films, electrochemical polymerization offers a number of benefits over chemical methods, including the ability to create polymer films on the electrode in a single step with high mechanical characteristics.. This eliminates the requirement for the film casting procedure and increases the pool of possible polymers.[33,34]

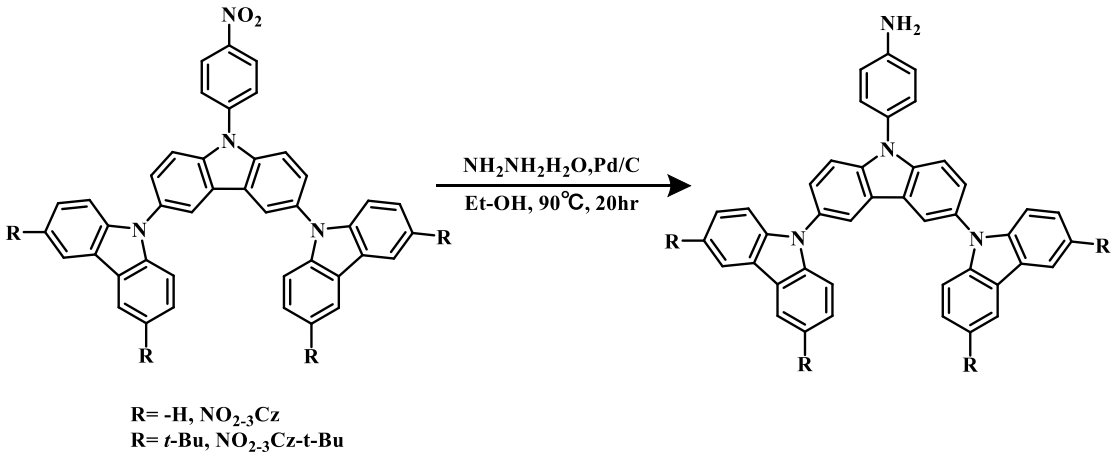

Figure 4.2 Synthetic procedure for 3,6-bis(*N*-carbazolyl)-*N*-phenylcarbazoles reported by Sheng *et al*. [22]

Two compounds, 3,6-di(carbazol-9-yl)-*N*-(4-nitrophenyl)carbazole tri-carbazole, 3,6-di(carbazol-9-yl)-*N*-(4-aminophenyl)carbazole (NH_2-3Cz), (3Cz) (NO_2-3Cz) were synthesized by Sheng *et al.*[22] and electro polymerized. The synthesized polymer films are deposited on the electrode surface in an electrolyte solution *via* the oxidative coupling reactions. The electro-generated polymer films exhibited reversible electrochemical oxidation processes, with a significant electrochromic behaviour. The P(NO_2-3Cz) film transitioned from a pale yellow neutral state to a yellow-green radical cation and finally to blue upon complete oxidation. The P(NH_2-3Cz) film turned from colourless to light green and then blue as a result of oxidation. Additionally, Sheng *et al*. described a few N-phenyl carbazoles with various phenyl group substituents. Possible processes of electropolymerization for the NO_2-3Cz and NH_2-3Cz monomers are proposed based on a comparative investigation. The former involves carbazole-carbazole coupling, while the latter involves both carbazole-carbazole and NH_2-carbazole couplings.

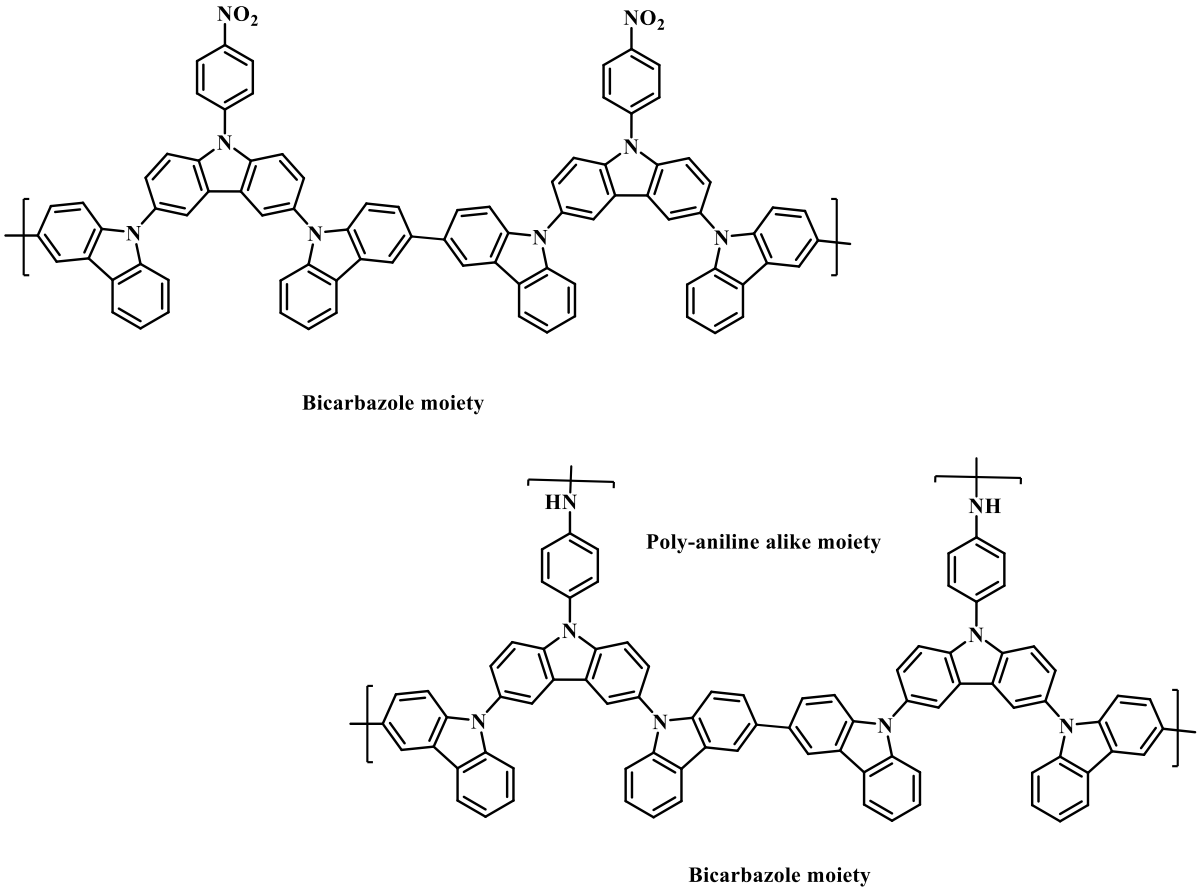

Figure 4.3 Structure of polymers synthesised by electrochemical polymerization reported by Sheng *et al.*[22]

The resultant P(NO_2 3Cz) polymer film displayed two reversible oxidation redox couples as a consequence of the oxidations of bicarbazole units, whereas the P(NH_2 3Cz) polymer film displayed multistep redox processes as a result of the biscarbazole and aminocarbazole moieties oxidations. During the oxidation processes, there were noticeable colour changes in both of the electrogenerated polymer films. Because of its polyanilinealike structure, the P(NH_2 3Cz) film exhibited a somewhat lower onset oxidation potential and stronger electrochromic stability than the P(NO_2 3Cz) film. The polymer films produced using electrogenous means have potential as materials for electrochromic uses.

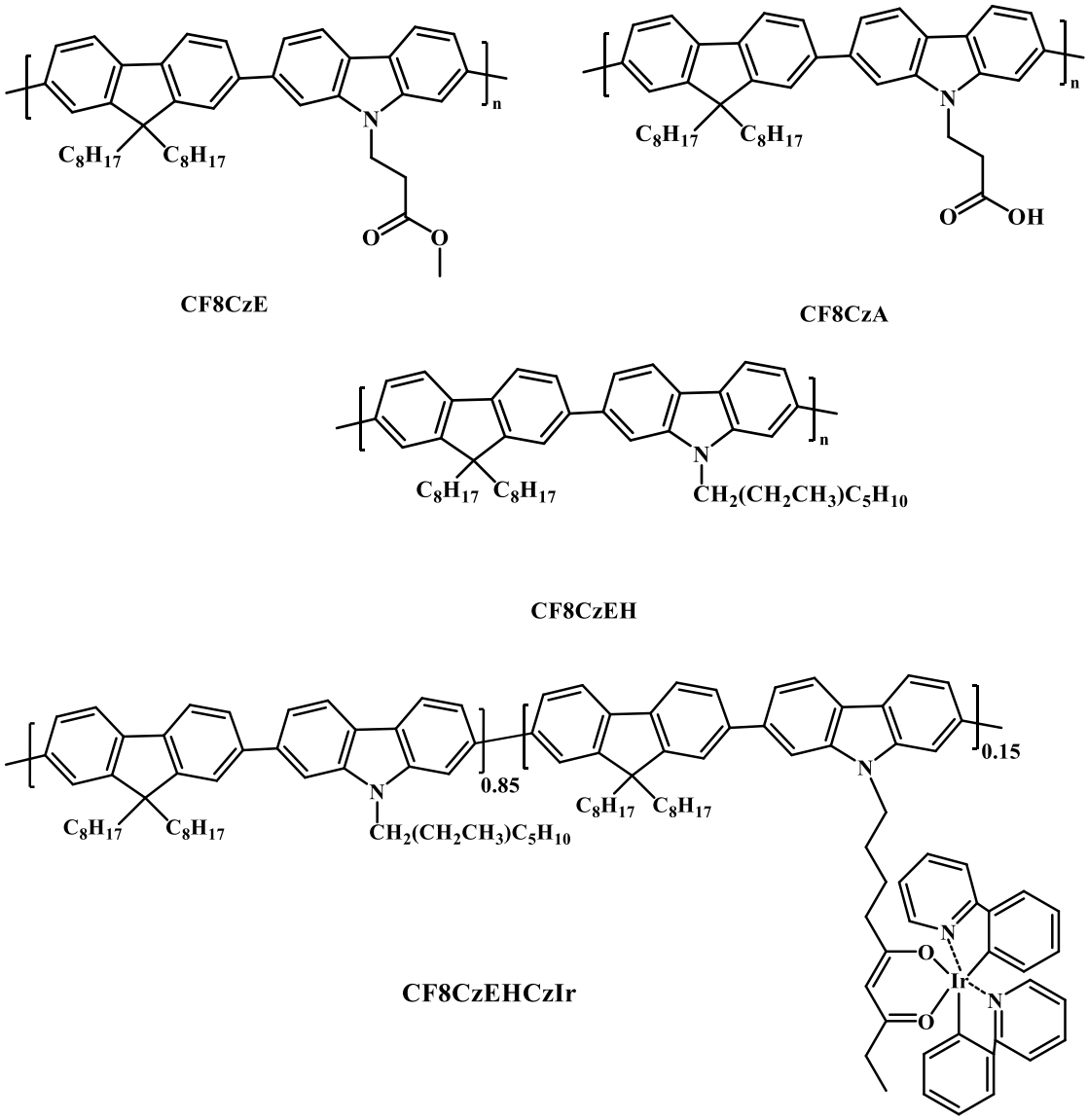

Figure 4.4 Structure of fluorene-carbazole based conjugated polymers reported by Cimrova *et al.*[35]

The carbazole-fluorene conjugated copolymers CF8CzE, CF8CzA, CF8CzEH, and CF8CzEHCzIr were synthesized by Cimrova *et al.*[35] via Suzuki coupling under various conditions, yielding copolymers with various average substituents in N-carbazole position 2-methoxycarbonylethyl, 2-carboxyethyl, 2-ethylhexyl, and nonan-2,4-dionatoiridium(III)bis(2-phenylpyridine N, C2′)-9-yl, respectively. The characteristics of carbazole units were found to be influenced by their molecular weight and the substituents connected to them containing the exception of the CF8CzEHCzIr copolymer containing iridium complex, the carbazole-fluorene copolymers showed strong photoluminescence (PL) emission in the blue spectral region of comparable spectral shapes with high PL quantum yields in diluted THF solutions. Greater disparities were seen between the thin-film PL, whose spectra are red-shifted, and electroluminescence (EL) spectra, which heavily rely on aggregation. It was discovered that the PL and EL processes are dominated by distinct centres. The best performing LEDs had low onset voltages, maximum EL efficiency, and efficient blue-white EL emission when constructed from CF8CzEH copolymers with a 2-ethylhexyl *N*-carbazole substituent. Together with memory effects that were more pronounced in LEDs composed of the lowest molecular weight copolymer, CF8CzE-3, and the CF8CzEHCzIr copolymer, LEDs composed of CF8CzE copolymers with 2-methoxycarbonylethyl and CF8CzEHCzIr copolymers showed a more notable anomalous current-voltage behaviour.

Such effects and behaviour could potentially be useful for photonic and bioinspired electrical applications in the future.

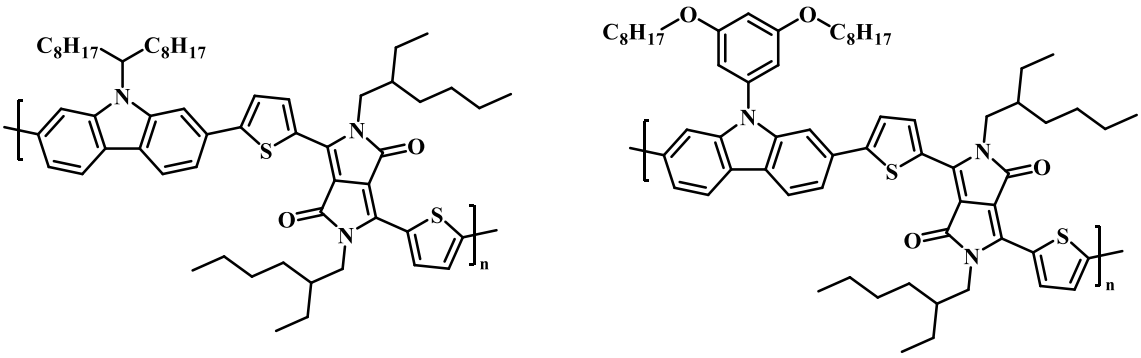

Figure 4.5 Structure of carbazole based conjugated polymers reported by Kwon *et al.*[36]

Two different types of novel conjugated copolymers based on carbazole and diketopyrrolopyrrole poly[*N*-9- heptadecanyl-2,7-carbazole-alt-5,5-(3,6-dithien-2-yl-2,5-bis(2-ethylhexyl)pyrrolo[*3,4-c*]pyrrole-1,4-dione)] (**P1**) and poly[*N*-9-(3,5-bis(octyloxy)phenyl)-2,7-carbazole-alt-5,5-(3,6-dithien-2-yl-2,5-bis(2-ethylhexyl) pyrrolo [*3,4-c*]pyrrole-1,4-dione)] (**P2**) was synthesized by Kwon *et al.*[36] by using Suzuki coupling reaction. The optical and electrical characteristics of these polymers, which had changed pendent groups on the carbazole moiety. As compared to alkyl substituted polymer **P1**, aryl substituted polymer **P2** exhibits a more planar backbone structure, a greater hole mobility (4.4 x 10^{-3} cm^2 V^1 s^1), and a smaller band gap (1.61 eV). Their surface morphologies were greatly altered by the side group modifications. Characterization was done on the device performance of solar cells based on these polymers and a fullerene acceptor.

In the present work, three new D-A type polymers, **TIIG-BP**, **THP-BP**, and **DAB-BP**, comprising three distinct π-extended iso-indigo units, were synthesised and characterized by NMR (^{1}H and ^{13}C). gel permeation chromatography (GPC), UV-visible spectroscopy, thermogravimetric analysis (TGA), powder X-ray diffraction analysis (PXRD), atomic force measurement (AFM) and electrochemical studies were performed to ascertain the characteristics of polymers. Additionally, space charge limit current (SCLC) hole mobilites of all the polymers were measured.

Results and discussion

9-Dodecyl-3,6-bis(4,4,5,5-tetramethyl-1,3,2-dioxaborolan-2-yl)-9*H*-carbazole was synthesised from carbazole *via* modified literature procedure reported by Gong *et al* and Sathiyan *et al.*[37,38]

Carbazole was subjected to n-alkylation using potassium hydroxide (KOH) and 1-bromododecane and the resulting products was reacted with N-bromo succinimide (NBS) and dimethyl formamide (DMF) to yield compound **2**. Borylation of compound **2** was carried out in presence of octamethyl-2,2'-bi(1,3,2-dioxaborolane) and tetrakis(triphenylphosphine) palladium (0) to yield compound **3**.

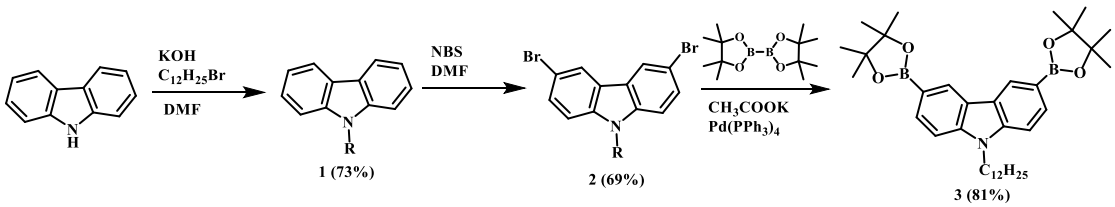

Scheme 4.1 Synthesis of 9-dodecyl-3,6-bis(4,4,5,5-tetramethyl-1,3,2-dioxaborolan-2-yl)-9*H*-carbazole (**3**)

Synthesis of monomers

Monomers, **M1**, **M2** and **M3** are synthesized from compound **4** using modified literature procedure.[39] The Knoevenagel condensation reaction was carried out between terephthaldehyde, compound **5** and thiophene-2,5-dicarbaldehyde with compound **4** in the presence of piperidine to yield three different monomers, **M1**, **M2** and **M3**.

The detailed experimental procedure of compound **4** and compound **5** are mentioned in chapter **2**.

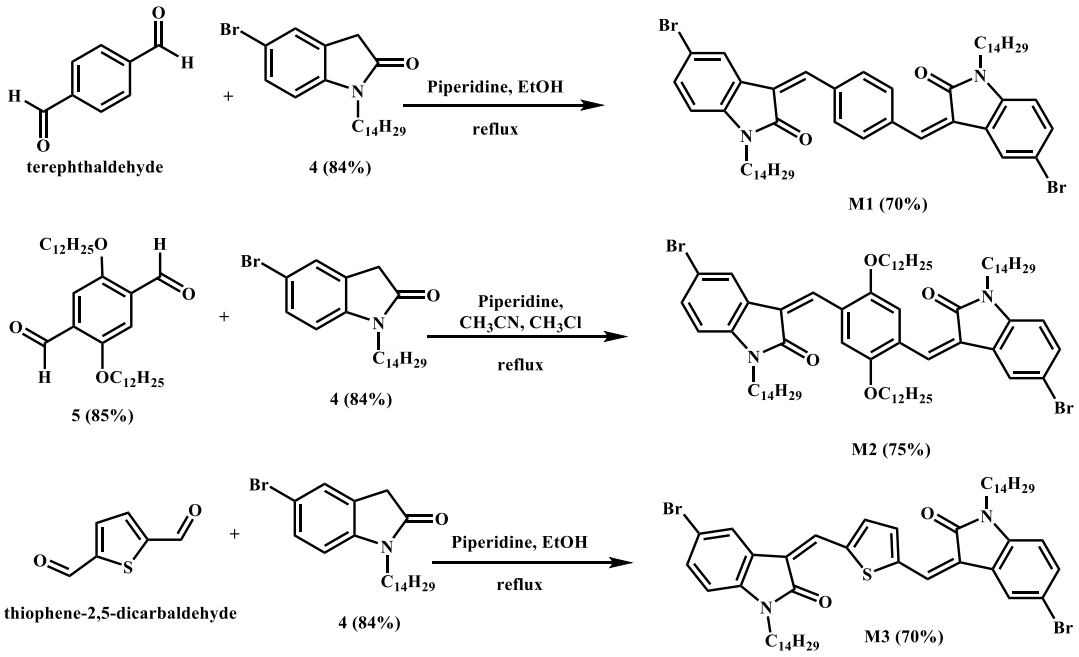

Scheme 4.2 Synthesis of monomers **M1**, **M2** and **M3.**

Synthesis of polymers

9-Dodecyl-3,6-bis(4,4,5,5-tetramethyl-1,3,2-dioxaborolan-2-yl)-9*H*-carbazole (**3**) is treated with three different monomers (**M1, M2** and **M3**) to get D-A-type π-conjugated polymers using a modified literature technique.[37,38] The compound (**3**) is subjected to Suzuki coupling reaction with three different monomers (**M1**, **M2**, and **M3**) in presence of tertakis (triphenylphosphine)palladium (0) ($Pd(PPh_3)_4$) and potassium carbonate (K_2CO_3) (Scheme 4.3).[3] The synthesized polymers are purified by Soxhlet extraction using methanol, petroleum ether, toluene, and chloroform. .

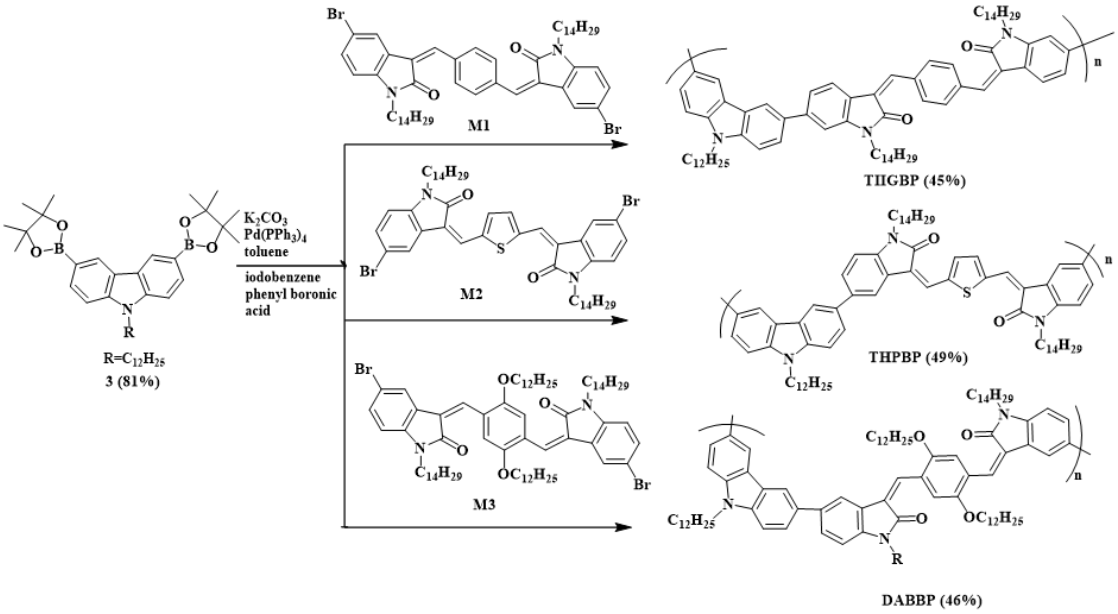

Scheme 4.3 Synthesis of carbazole based D-A-type conjugated polymers, **TIIG-BP**, **THP-BP** and **DAB-BP**.

Molecular weight and thermal properties of polymers

The decomposition temperature (T_d), average molecular weights (M_n and M_w) and polydispersity index (Đ) of polymers, **TIIG-BP**, **THP-BP** and **DAB-BP** are summarized in Table 4.1. The average molecular weights of the polymers are calculated by gel permeation chromatography (GPC) analysis. The data obtained from GPC analysis showed that the chain length of polymers was 12, 18 and 18 comonomer units for polymers, **TIIG-BP**, **THP-BP** and **DAB-BP**, respectively.

Thermogravimetric analysis is used to evaluate the thermal characteristics of all three polymers at a heating rate of 10 ℃/min in a nitrogen atmosphere. The temperature at which polymer loses 5% of its weight is considered as the decomposition temperature (T_d). The synthesized polymers have decomposition temperatures above 340 ℃, indicating that their thermal stabilities are high enough for use in organic electrical devices. The thermal breakdown temperature (T_d) of polymers, **TIIG-BP**, **THP-BP** and **DAB-BP** (Figure 4.6; black, red, and blue lines, respectively) is 346 ℃, 360 ℃, and 342 ℃.

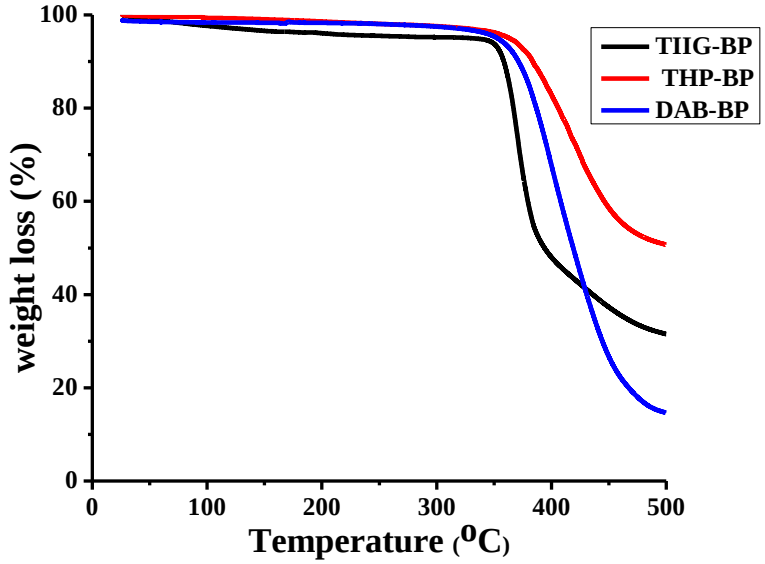

Figure 4.6 Thermogravimetric analysis (TGA) of π-extended D-A-type conjugated polymers, **TIIG-BP** (black line), **THP-BP** (red line) and **DAB-BP** (blue line).

Photophysical properties of polymers

UV-visible spectroscopy of diluted chloroform solutions (10^{-6} μM) was used to study the photophysical properties of the polymers, **TIIG-BP**, **THP-BP** and **DAB-BP**. Multiple band absorption spectra with intricate band splitting patterns were displayed by all three polymers, **TIIG-BP**, **THP-BP** and **DAB-BP**. Figure 4.7 illustrates that the polymers, **TIIG-BP**, **THP-BP** and **DAB-BP,** have broad absorption spectra that are due to the π-π* transitions. The absorption bands (λmax) are located at 293 nm, 252 nm and 257 nm, respectively. The polymer **THP-BP** was found to have a shoulder peak in its first absorption band at 293 nm. The second band in the polymer **TIIG-BP** absorption spectra, which has an absorption maximum (λmax) at 390 nm, which might be the result of intramolecular charge transfer (ICT). The peaks observed at 451 nm and 458 nm for polymers, **THP-BP** and **DAB-BP**, are due to the similar ICT effect. For polymers **DAB-BP**, the CT transition band shoulder peak was measured at 357 nm. The optical band gap for polymers, **TIIG-BP**, **THP-BP,** and **DAB-BP**, were determined at 505, 606, and 570, respectively, based on the absorption edge (λ_{edge}) of synthesised polymers. The band gap value of polymers, **TIIG-BP**, **THP-BP,** and **DAB-BP** were found to be 2.45 eV, 2.04 eV, and 2.17 eV, respectively. The photophysical properties of the synthesized polymers were summarized in Table 4.1.

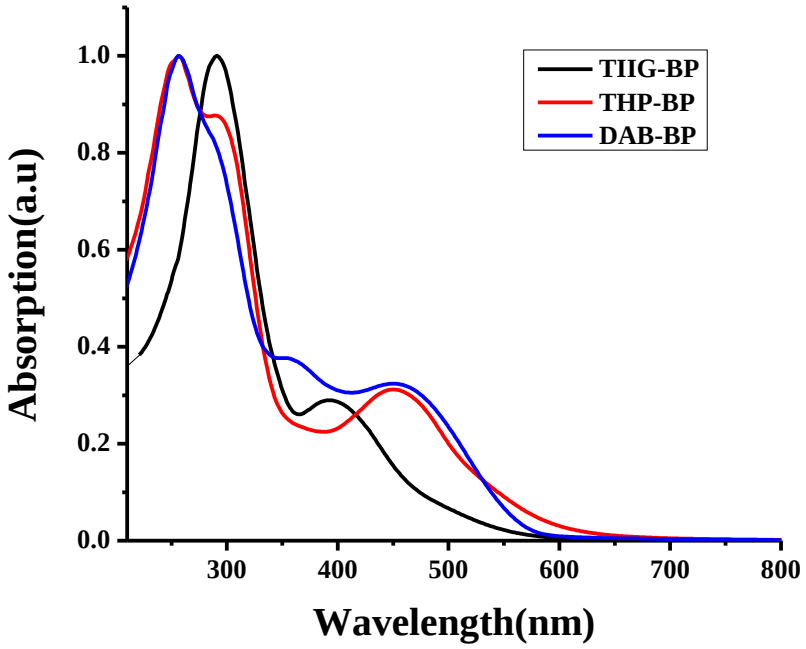

Figure 4.7 Absorption spectra of conjugated polymers, **TIIG-BP** (black line), **THP-BP** (red line) and **DAB-BP** (blue line).

Table 4.1 Photophysical properties, thermogravimetric analysis (TGA) and Gel permeation chromatography (GPC) analysis of polymers, **TIIG-BP**, **THP-BP** and **DAB-BP**

Compound	λ_{max} (nm)	λ_{edge} (nm)	E_g^{opt} (eV)[a]	T_d (^oC)[b]	M_w (Dalton)[c]	PDI (Đ)[c]
TIIG-BP	293, 390	505	2.45	349	12827	1.72
THP-BP	252, 451	606	2.04	238	18703	1.69
DAB-BP	257, 458	570	2.17	265	18480	1.75

[a]Calculated using equation $E_g^{opt} = 1240/\lambda_{edge}$, [b]Decomposition temperature T_d (obtained from TGA), [c]Molecular weight M_w and poly-dispersity index (Đ, obtained from GPC analysis);

Electrochemical properties of polymers

The frontier orbital energy levels of conjugated polymers, **TIIG-BP**, **THP-BP** and **DAB-BP** are determined by means of cyclic voltammetry (CV). Tetra-n-butylammonium hexafluorophospate ($TBAPF_6$) is used as a supporting electrolyte (~50 mM) in CV experiments conducted in the dry acetonitrile-chloroform (7:3) solution.

Using a three-electrode system, the working electrode is a Pt disc electrode, the counter electrode is a Pt wire electrode, and the reference electrode is Ag/Ag^{+}. In a dry acetonitrile-chloroform (7:3) solution (5 mM), the polymers **TIIG-BP**, **THP-BP**, and **DAB-BP** are dissolved, followed by degas with nitrogen gas.

The CV (Figures 4.8 a, b, and c) exhibit irreversible oxidation in all polymers. Polymers, **TIIG-BP**, **THP-BP** and **DAB-BP** have oxidation potentials of +0.48 V, +0.50 V, and +0.48 V, respectively. The polymers, **TIIG-BP**, **THP-BP** and **DAB-BP** exhibit onset oxidation potentials at +0.36 V, +0.41 V, and +0.38 V, respectively. These potential are determined by measuring the oxidation waves (Figure 4.8 a, b, and c). Utilising the onset oxidation potentials, the corresponding HOMO energy levels are determined to be 4.66 eV, 4.71 eV, and 4.68 eV, The LUMO energy levels of polymers, **TIIG-BP**, **THP-BP**, and **DAB-BP** are found to be −2.21 eV, −2.67 eV and −2.51 eV, respectively, by applying the formula $E_{LUMO} = E_{HOMO} + E_g^{opt}$. Table 4.2 provides an overview of the polymers' electrochemical characteristics.

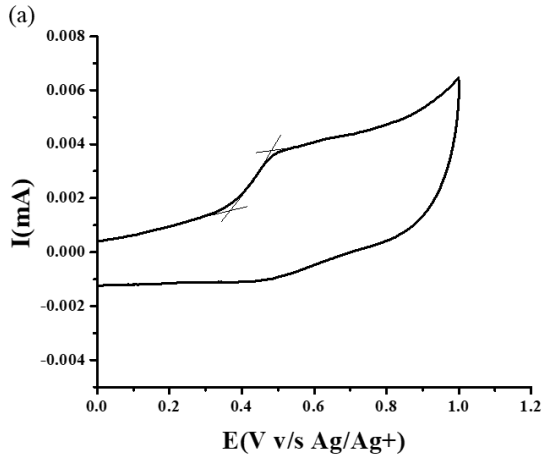

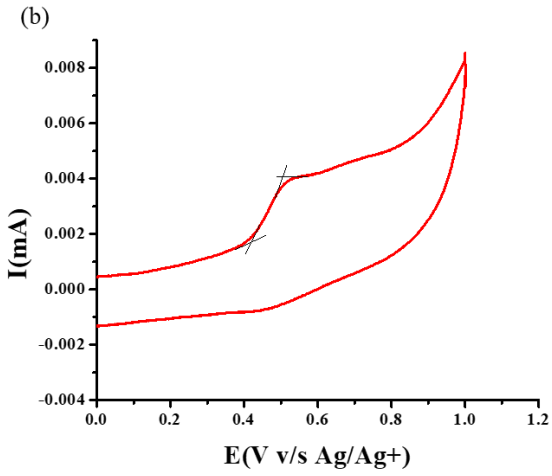

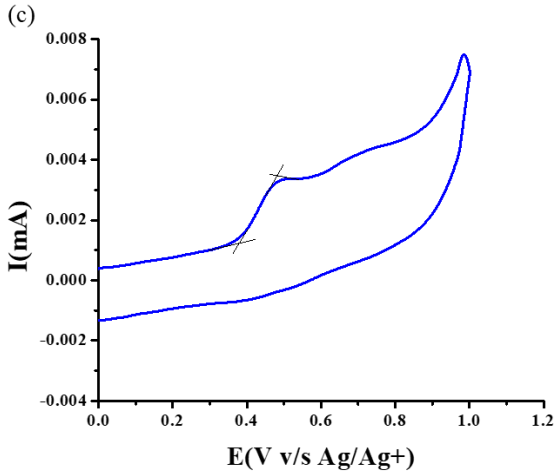

Figure 4.8 Oxidation curves of polymers, (a) **TIIG-BP** (b) **THP-BP** and (c) **DAB-BP** obtained by cyclic voltammetry at 50 mV/s in dry acetonitrile-chloroform (7:3) using $TBAPF_6$ as a supporting electrolyte; $\boldsymbol{E_{onset\ Fc/Fc^+} = 0.50\ V}$.

Table 4.2 Electrochemical properties of conjugated polymers **TIIG-BP**, **THP-BP** and **DAB-BP**.

Compound	E_{oxi} (V) [a]	$E_{oxi,onset}$ (V) [a]	E_{HOMO} (eV) [b]	E_{LUMO} (eV) [c]
TIIG-BP	+0.48	+0.36	−4.66	−2.21
THP-BP	+0.50	+0.41	−4.71	−2.67
DAB-BP	+0.48	+0.38	−4.68	−2.51

[a]potential v/s Ag/Ag^+; [b]calculated from equation $\boldsymbol{E_{HOMO} = -(E_{onset\ oxi} + 4.8 - E_{onset\ Fc/Fc^+})}$; [c]calculated from equation $\boldsymbol{E_{LUMO} = E_{HOMO} + E_g^{opt}}$.

X-ray diffraction studies of polymers

The powder X-ray diffraction (PXRD) analysis of polymer films, specifically **THP-BP**, **DAB-BP**, and **TIIG-BP**, is shown in Figure 4.9. Each of these films exhibits a significant broad peak near 2Θ at 20.81° and a minor peak at 39.59°. These observations indicate that the polymers are amorphous and share a similar structural characteristic.[40]

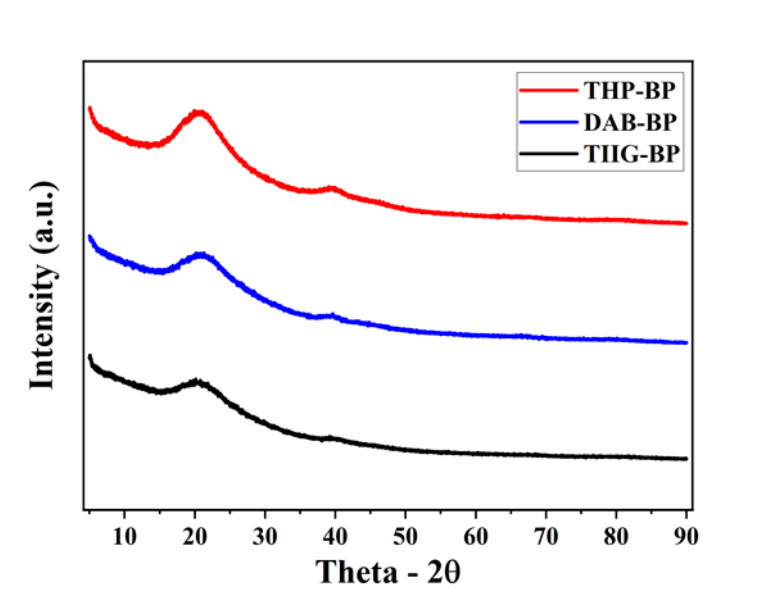

Figure 4.9 Powder X-ray diffraction pattern spectra of polymers, **TIIG-BP, THP-BP** and **DAB-BP**.

Atomic Force Microscopy (AFM) analysis

Tapping mode atomic force microscopy (AFM) was employed to examine the morphological features of a Polymer/NiOx/FTO film. As shown in Figure 4.10, the polymer **THP-BP** has the lowest root mean square (RMS) roughness value at 3.98 nm, setting it apart from the other polymers. In contrast, the RMS roughness values for polymers, **DAB-BP** and **TIIG-BP** are 6.12 nm and 15.59 nm, respectively.

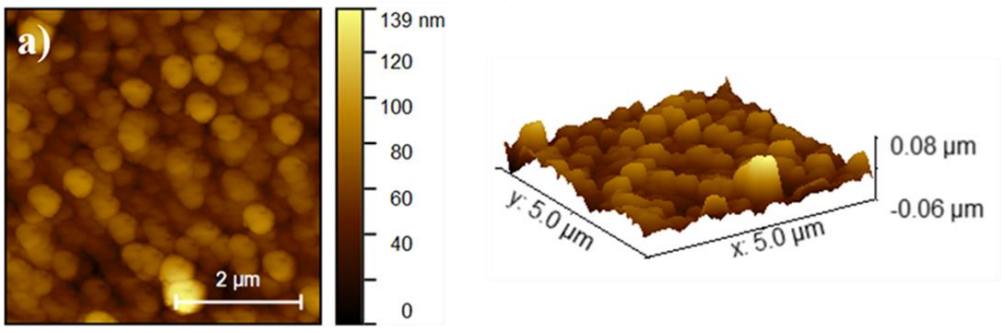

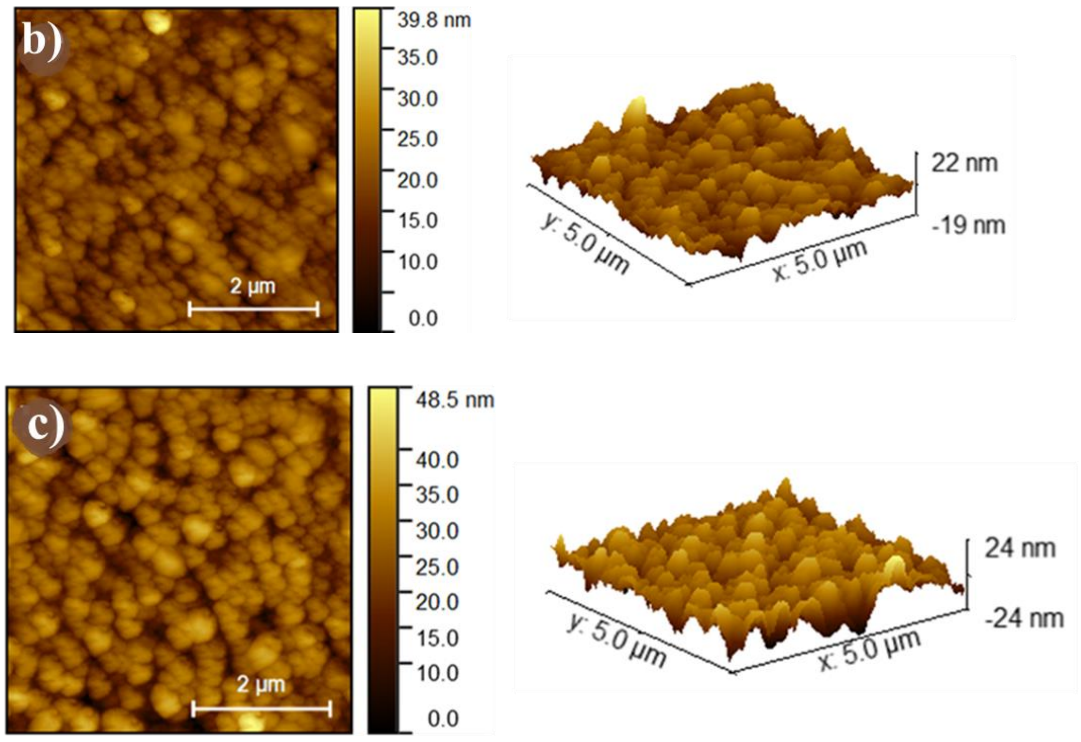

Figure 4.10 AFM images of polymer films (a) **TIIG-BP**, (b) **DAB-BP** and (c) **THP-BP.**

Space Charge Limited Current (SCLC) measurement of polymers

The hole mobilities in polymers were determined using the Mott-Gurney equation, which connects current density (J) to applied voltage (V) and film thickness (L) through the dielectric properties of the material. In this equation, ε_0 represents the vacuum permittivity (8.85×10^{-12} Fm^{-1}), and εr is the dielectric constant, typically assumed to be 3 for organic semiconductors. This allows for the calculation of hole mobility (μ), providing a quantitative assessment of charge carrier transport characteristics within the material. This application of fundamental electrostatic principles highlights the precise scientific method employed to elucidate charge carrier dynamics in polymer-based electronic systems.[41–43]

$$J = \frac{9}{8}\varepsilon_r\varepsilon_0\mu\frac{V^2}{L^3}$$

where, J is the current density, μ is the hole mobility, ε_o is the vacuum permittivity (8.85 × 10^{-12} Fm^{-1}), ε_r is the dielectric constant of the material (considered as 3 for organic semiconductors), L is the film thickness, and V is the applied voltage.

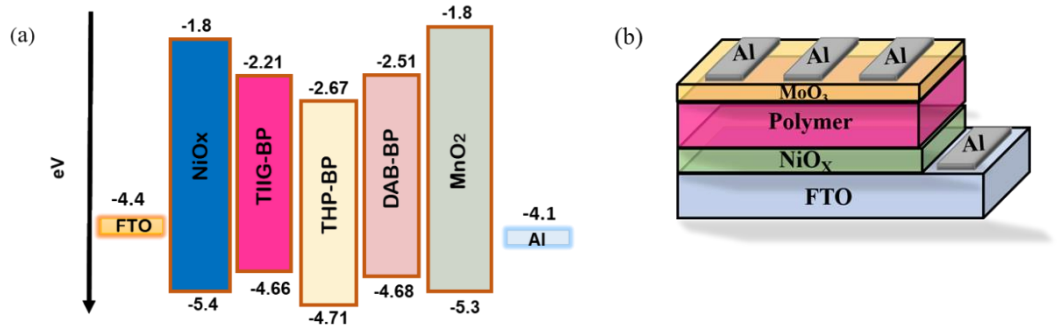

Figure 4.11 (a) The energy level diagram of polymers, **TIIG-BP, THP-BP** and **DAB-BP** (b) Schematic diagram of a hole-only device.

The hole mobility in the synthesized polymers was evaluated using the Space Charge Limited Current (SCLC) technique within a hole-only device structure, described as FTO/NiOx/Polymer/MoO_3/Al, with an active area of 0.12 cm^2 (Figure 4.11). To ensure the substrates were pristine, the FTO glass slides were meticulously cleaned by sonication in a soap solution, followed by sequential rinsing with deionized water, acetone, and isopropyl alcohol, each for 15 minutes. After cleaning, the FTO slides were subjected to UV-ozone treatment.

The NiOx precursor solution was evenly spin-coated onto the FTO glass surface at 3500 rpm for 45 seconds, followed by annealing at 300 °C for 1 hour to form a hole transport layer (HTL) approximately 120 nm thick. Next, the polymer solution, dissolved in chloroform, was spin-coated onto the substrate at 1000 rpm for 60 seconds. This was followed by thermal annealing at 80 °C for 10 minutes to ensure proper film formation.

A 20 nm thick layer of molybdenum trioxide (MoO_3) was thermally deposited as a buffer layer. Subsequently, 100 nm thick aluminium (Al) metal electrodes were deposited using a shadow mask. Current density-voltage characteristics were measured with a CHI660E instrument at a scan rate of 100 mV s^{-1}, enabling comprehensive characterization of the device performance.

The determination of hole mobilities was carried out by extracting data from the linear region of the Log J versus Log V curve, as shown in Figure 4.12. The measured

hole mobilities for the polymers, **TIIG-BP**, **DAB-BP** and **THP-BP** were found to be 1.25×10^{-2}, 2.45×10^{-2}, and 5.21×10^{-2} $cm^2V^{-1}s^{-1}$, respectively. This analytical method allowed for precise quantification of charge carrier mobility within the fabricated devices, providing valuable insights into the electronic transport properties of the respective polymer materials.[41–43]

The significant enhancement in hole mobility observed in polymer **THP-BP**, compared to the other polymers, can likely be attributed to its notably smoother surface morphology. This increased surface smoothness is thought to enhance the efficiency of charge transfer pathways at the interfaces, thereby improving charge transfer dynamics across the various layers. This phenomenon underscores the critical role of surface morphology in determining charge transport properties within the device architecture, providing crucial insights into the mechanism governing charge carrier mobility enhancement in polymer-based electronic systems.[43,44]

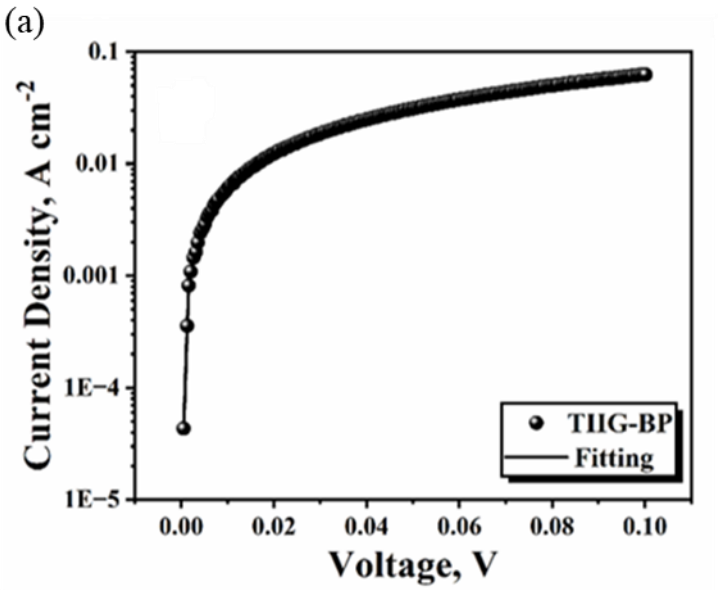

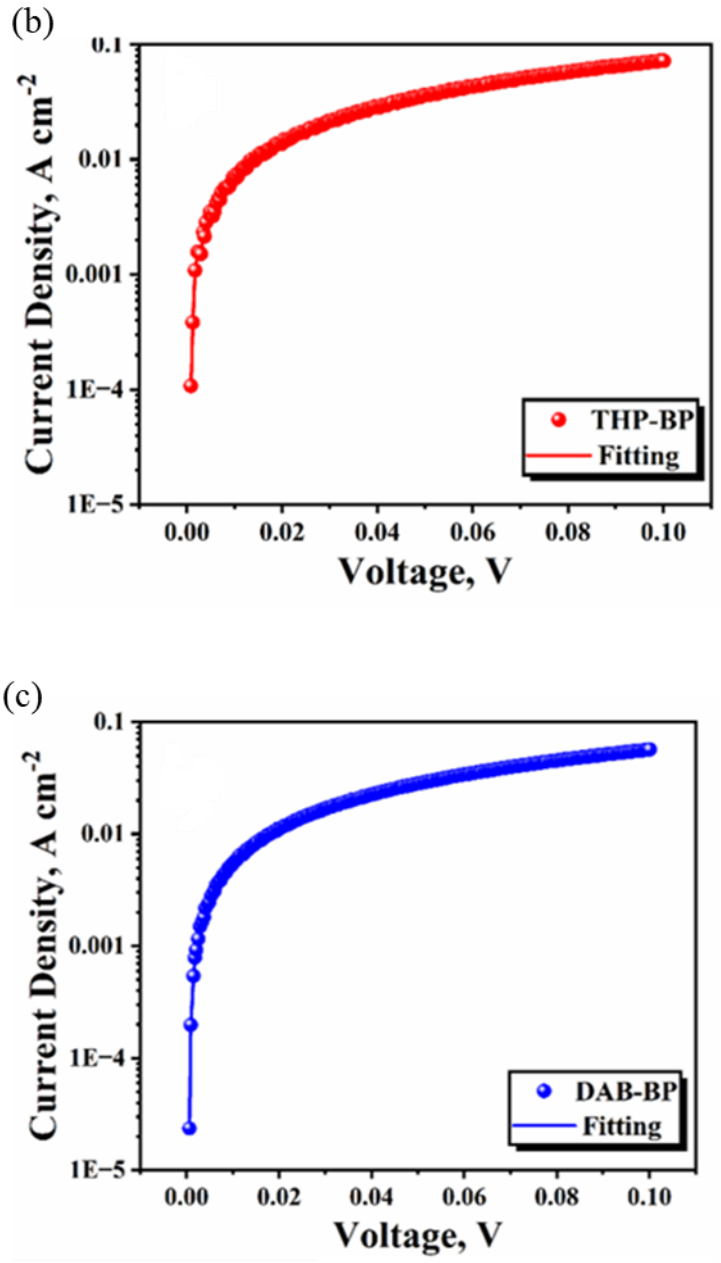

Figure 4.12 SCLC hole mobilities of **TIIG-BP**, **DAB-BP** and **THP-BP** polymers.

Conclusion

The polymerization of borylated carbazole was conducted using three distinct π-extended isoindigo units with the assistance of a Pd catalyst. NMR, UV-Visible, GPC, TGA and electrochemical studies were used to thoroughly characterise the synthesised polymers. The photophysical characteristics of **TIIG-BP**, **THP-BP** and **DAB-BP** revealed wide absorption spectra, and the corresponding band gap values were determined to be 2.45 eV, 2.04 eV, and 2.17 eV. All the conjugated polymers demonstrated adequate high thermal stability along with moderate to good solubility in standard organic solvents. According to the GPC study, the chain lengths of polymers **TIIG-BP**, **THP-BP**, and **DAB-BP** were 12, 18, and 18 comonomer units, respectively. All polymers were shown to be fairly stable up to 340 °C by thermogravimetric analysis (TGA). The HOMO energy were found to be below -5.0 eV for all the polymers. The LUMO energy levels of polymers were found to be in the range of -2.67 eV to -2.21 eV. The powder X-ray diffraction (PXRD) analysis of polymers, **TIIG-BP**, **THP-BP**, and **DAB-BP** shows that all the polymers are amorphous in nature. The atomic force microscopy (AFM) of all the three polymers were carried out and the AFM data conclude that **THP-BP** has the lowest root mean square (RMS) roughness value at 3.98 nm. The Space Charge Limited Current (SCLC) hole mobilities for the polymers **TIIG-BP**, **DAB-BP**, and **THP-BP** were found to be 1.25×10^{-2}, 2.45×10^{-2}, and 5.21×10^{-2} $cm^2V^{-1}s^{-1}$, respectively. The preliminary characterization data showed that the new synthesized conjugated polymers, **TIIG-BP**, **THP-BP** and **DAB-BP** were potential candidates for organic electronic devices.

Experimental procedures

General procedure

All the chemicals are reagent grade and are used as purchased. Moisture sensitive reactions are performed under inert atmosphere under dry nitrogen by using dry solvents. Reactions are monitored by thin-layer chromatography (TLC) using Merck 60 F254 aluminium-coated plates and the spots are visualized under ultraviolet (UV) light. Column chromatography is carried out on silica gel (60–120 mesh).

^{1}H and ^{13}C NMR spectra are recorded on a Bruker Avance-III 400 spectrometer in $CDCl_3$ and DMSO-D6. The high resolution mass spectra are recorded on Xevo G2-XS QTOF Mass Spectrometer. Thermogravimetric analysis (TGA) is done on Exstar SII TG/DTA 6300 using N_2 as an inert gas. Molecular weights of the polymer samples are measured with Agilent 1260 Infinity GPC instrument, equipped with RI detector. Polystyrene is used as a calibration standard. Polymer sample (~5 mg) are dissolved in THF (~5 mL) and are filtered through a 0.2 µ filter. The analysis is done using THF as an eluent at a flow rate of 1-2 mL/min. UV-Visible absorption spectra are recorded on Jasco FP 6300 spectrofluorometer using quartz cuvette. Electrochemical studies are carried out by using an Electro Chemical Analyser, Model SP-200, Biologics Sas France Make using platinum (Pt) disk electrode as a working electrode, platinum wire as a counter electrode and AgCl-coated Ag wire as a reference electrode. Non-aqueous Ag/Ag^{+} wire is prepared by dipping silver wire in a solution of $FeCl_3$ and HCl. Pt-disk electrodes were polished with alumina and washed with water and acetone and were dried with nitrogen gas before use to remove any incipient oxygen. All electrochemical potentials are reported against Ag/Ag^{+} taking ferrocene as an external standard; $E_{(onset(Fc/Fc)+)} = 0.50$ V

Synthesis of 9-dodecyl-3,6-bis(4,4,5,5-tetramethyl-1,3,2-dioxaborolan-2-yl)-9*H*-carbazole

Compound **3** was synthesized according to the modified literature procedure reported by Gong *et al* and sathiyan *et al.*[37,38]

Synthesis of 9-methyl-9*H*-carbazole (1): Carbazole (1 g, 5.98 mmol, 1 eq), potassium hydroxide (0.9 g, 15 mmol, 2.5eq), dissolved in DMF (15 mL) and then n-dodecyl bromide (1.49 g, 5.98 mmol, 1.1 eq) was added dropwise. The reaction mixture was

stirred at room temperature for 48 h. The reaction mixture was poured in to water, extracted with ethyl acetate and dried over sodium sulphate. The solvent was removed by distillation and the crude was purified by column chromatography by using 10% ethyl acetate petroleum ether as mobile phase.

9-Methyl-9*H*-carbazole (1): (2.47g, 92%) ^{1}H NMR (400 MHz, $CDCl_3$): δ 8.16-8.18 (d, 2H), 7.50-7.54 (m, 2H), 7.45-7.47 (d, 2H), 7.23-7.34 (m, 2H), 4.32-4.35 (t, 2H), 1.88-2.42 (2H), 1.30-1.57(m, 12H), 0.91-0.94 (4H).

Synthesis of 3,6-dibromo-9-dodecyl-9*H*-carbazole (2): In to a two necked round bottom flask compound **1** (1.5g, 8.9mmol, 1eq) was dissolved in dry DMF (20 mL). The solution was allowed to cooled at 0 ℃ and a solution of NBS (3.2 g, 17.80 mmol, 2.2 eq) in DMF (10 mL) was added dropwise under nitrogen atmosphere. After the addition was completed the reaction mixture was allowed to stir at room temperature for 12 h. The reaction mixture was poured in to water (250 mL) and the resulting white precipitate was filtered. The crude was dissolved in chloroform and washed with water to remove water soluble impurities, dried over sodium sulphate, filtered and concentrated under reduced pressure. The crude product was recrystallized by using ethanol.

3,6-Dibromo-9-dodecyl-9*H*-carbazole (2): (2.47g, 76%) ^{1}H NMR (400 MHz, $CDCl_3$): δ 8.33 (s, 1H), 7.71-7.73 (s, 1H), 7.17-7.19 (s, 1H), 4.20-4.24 (s, 1H), 1.80-1.83 (s, 2H), 1.23-1.31 (m, 11H), 0.89-0.91 (s, 2H).

Synthesis of 9-dodecyl-3,6-bis(4,4,5,5-tetramethyl-1,3,2-dioxaborolan-2-yl)-9*H*-carbazole (3): In to a two necked round bottom flask compound **2** (0.8 g, 1.3mmol, 1eq) and DMF (20 mL) was added and the reaction mixture was stirred to dissolve the compound. Bispinacolato diborane (1 g, 3.9mmol, 3 eq) and potassium acetate (0.5 g, 5.2 mmol, 4 eq) was added to the reaction mixture after that the reaction mixture was purged with nitrogen for 15 min. $Pd(PPh_3)_2Cl_2$ (0.09 g, 0.13 mmol, 0.1 eq) was added to the reaction mixture. The reaction mixture was heated at 130 ℃ for 36 h under nitrogen atmosphere. After completion of the reaction, the reaction mixture was poured in to water and the crude product was extracted with ethyl acetate. The organic layer was washed with water, brine, dried over sodium sulphate and concentrated under reduced pressure. The crude product was purified by column chromatography using 10% ethyl acetate – petroleum ether system.

9-Dodecyl-3,6-bis(4,4,5,5-tetramethyl-1,3,2-dioxaborolan-2-yl)-9*H*-carbazole (3): (2.47g, 81%) ^{1}H NMR (400 MHz, $CDCl_3$): δ 8.68 (s, 2H), 7.90-7.93 (s, 2H), 7.40-7.42 (s, 2H), 4.30-4.33 (s, 2H), 1.82-1.88 (s, 3H), 1.23-1.80 (s, 31H), 0.37-0.91 (m, 15H).

Synthesis of monomers

Synthesis of (3Z,3'Z)-3,3'-(1,4-phenylenebis(methaneylylidene)) bis(5-bromo-1-tetradecylindolin-2-one) (M1): In 22 mL of absolute ethanol, terephthalaldehyde (0.041 g, 0.30 mmol) and compound **4** (0.20 g, 0.16 mmol) were added under nitrogen atmosphere. To this stirred solution, piperidine (0.1 mL, 1.07 mmol) was added drop wise and reaction mixture was allowed to reflux for 24 h. After that, the reaction mixture was cooled to room temperature and the precipitated product is collected by filtration. The filtered product was washed with copious amount of absolute ethanol and dried at room temperature. The pure product was obtained by re-crystallization from petroleum ether-chloroform solution.

Compound **M1**: Dark orange solid (0.14g, 65%) ^{1}H NMR (400 MHz, $CDCl_3$): 8.38 (s, 2H), 7.64 (d, J3 = 2.0 Hz, 1H), 7.49 (s, 1H), 7.36 (dd, J2 = 8.0 Hz, J3 = 1.6 Hz, 1H), 6.68 (d, J2 = 8.4 Hz, 1H), 3.69−3.73 (t, J2 = 7.6 Hz, 2H), 1.68−1.73 (m, 2H), 0.95−0.98 (t, J2 = 7.6 Hz, 3H). ^{13}C NMR (100 MHz, $CDCl_3$): δ 165.3, 140.9, 137.1, 135.6, 132.2, 131.5, 126.2, 122.4, 114.4, 109.6, 40.1, 31.9, 29.5, 29.3, 27.5, 22.7, 14.1.

Synthesis of (3Z,3'Z)-3,3'-(thiophene-2,5-diylbis(methaneylylidene)bis(5-bromo-1-tetradecylindolin-2-one) (M2): To a 100 mL round bottom flask, compound **5** (0.35g, 0.61mmol) and compound **4** (0.5g, 1.22mmol)) in acetonitrile (15 mL) and chloroform (15 mL) were added and stir at room temperature. The reaction mixture was degassed by purging nitrogen gas. To this stirred solution piperidine (0.18g, 2.13mmol) was added drop wise and the reaction mixture was allowed to reflux for 24h. After that, the reaction mixture is cooled to room temperature and the precipitated product was collected by filtration. The filtered product was washed with copious amount of acetonitrile and dried at room temperature. The pure product was obtained by re-crystallization from petroleum ether-chloroform solution.

Compound **M2**: Dark red solid (0.5g, 75%), ^{1}H NMR (400MHz, $CDCl_3$) δ: 8.81 (s, 2H), 8.01 (s, 2H) 7.60 (d, J3=4.0 Hz, 1H) 7.34 (dd, J2=8.0Hz, 1H), 6.66 (d, J2=8Hz,

1H), 4.18 (t, J2=8Hz 2H), 3.71 (d, J2=8Hz), 1.57 (m, 6H), 1.24-1.32 (m, 41H), 0.84-0.87 (m, 9H), ^{13}C NMR (100 MHz, $CDCl_3$): δ 165.7, 152.1, 140.4, 131.8, 131.0, 127.0, 126.8, 124.8, 122.3, 115.1, 114.3, 109.3, 40.0, 31.9, 29.7, 26.6, 22.12, 14.16.

Synthesis of (3Z,3'Z)-3,3'-((2,5-bis(dodecyloxy)-1,4-phenylene) bis (methaneylylidene)) bis(5-bromo-1-tetradecylindolin-2-one) (M3): To a 100 mL round bottom flask, take thiophene 2,5-dicarboxyaldehyde (0.12g, 0.85mmol) and compound **4** (0.7g, 1.75mmol) in acetonitrile (15 mL) and chloroform (15 mL) were stir at room temperature. The reaction mixture was degassed by purging nitrogen gas. To this stirred solution piperidine (0.25g, 3.0mmol) was added drop wise and the reaction mixture was allowed to reflux for 24h. After that, the reaction mixture was cooled to room temperature and the precipitated product was collected by filtration. The filtered product was washed with copious amount of acetonitrile and dried at room temperature The pure product was obtained by re-crystallization from petroleum ether-chloroform solution.

Compound **M3**: Brown solid (0.64g, 70%), ^{1}H NMR (400 MHz, $CDCl_3$) δ: 8.09 (s, J2=16Hz, 1H), 7.90 (s, 1H), 7.53 (s, 1H), 7.53 (dd, J3=8Hz,1H), 7.2 (s, 1H), 6.65 (dd, J3=8Hz, 1H), 3.75 (d J2=12Hz, 2H), 1.60-1.69 (d, 3H), 1.07-1.33 (m, 23H), 0.70-0.87 (d, 3H), ^{13}C NMR (100 MHz, $CDCl_3$): δ 143.8, 140.6, 137.1, 131.4, 127.7, 125.6, 122.1, 114.3, 109.6, 40.1, 31.9, 29.7, 29.6, 29.5, 29.3, 27.6, 22.7.

Synthesis of polymers

9-Dodecyl-3,6-bis(4,4,5,5-tetramethyl-1,3,2-dioxaborolan-2-yl)-9*H*-carbazole is coupled with three different π-extended D-A type iso-indigo based monomers in presence of potassium carbonate (K_2CO_3), tertakis(triphenylphosphine)palladium (0) ($Pd(PPh_3)_4$), phenyl boronic acid and iodobenzene in refluxing toluene. The detailed experimental procedure is mentioned below.[37,38]

General procedure for synthesis of carbazole based conjugated polymers TIIG-BP, THP-BP and DAB-BP

In a dry three-neck round bottom flask attached with condenser under nitrogen atmosphere, compound **M1** (0.1 g, 0.109 mmol, 1 eq), compound **M2** (0.1 g, 0.108 mmol, 1 eq) or compound **M3** (0.1g, 0.214mmol, 1 eq) was dissolved in 30 mL dry

toluene. To this solution 9-dodecyl-3,6-bis(4,4,5,5-tetramethyl-1,3,2-dioxaborolan-2-yl)-9*H*-carbazole (**3**) (1.1 eq) and potassium carbonate (3 eq) dissolved in degassed water were added. The reaction mixture was allowed to purged with nitrogen for 20 min, after that $Pd(PPh_3)_4$ (0.1 eq) was added and the reaction mixture was allowed to reflux for 72h. After 72h, iodobenzene was added to the reaction mixture and the reaction mixture was refluxed for 3 h, followed by the addition of phenylboronic acid and refluxed for three more hours. After completion of reaction, the excess solvent was removed under vacuum, and the crude polymer was dissolved in chloroform. The organic layer was washed with water and brine, dried over sodium sulphate and concentrated. The concentrated solution was poured into 300 mL methanol and left overnight to precipitate out. The precipitate was filtered off, washed with methanol and dried. To remove the lower molecular weight fraction, the precipitate was purified by Soxhlet extraction using petroleum ether, toluene and chloroform.

TIIG-BP: Red colour polymer obtained with 49% yield. ^{1}H NMR (400 MHz, $CDCl_3$): δ 7.87-7.90 (m, 9H), 7.28-7.41 (m, 9H), 4.72-4.76 (7H), 2.11-2.15 (m, 7H), 1.25-1.44 (m, 154H), 0.87-0.91(m, 45H).

THP-BP: Brown colour polymer obtained with 53% yield. ^{1}H NMR (400 MHz, $CDCl_3$): δ 7.95-8.71 (m, 8H), 7.47-7.91 (m, 8H), 4.0-4.38 (m, 3H), 3.47-4.03 (m, 5H), 1.70-1.74(20H), 1,35-1.44 (160H),

DAB-BP: Dark red colour polymer obtained with 53% yield. ^{1}H NMR (400 MHz, $CDCl_3$): δ 7.91-8.14 (m, 8H), 7.50-7.64 (7H), 3.78-4.22 (7H), 1.30-1.60 (m, 34H), 1.10-1.27 (m, 130H), 0.86-0.89 (m, 73H).

Spectral data

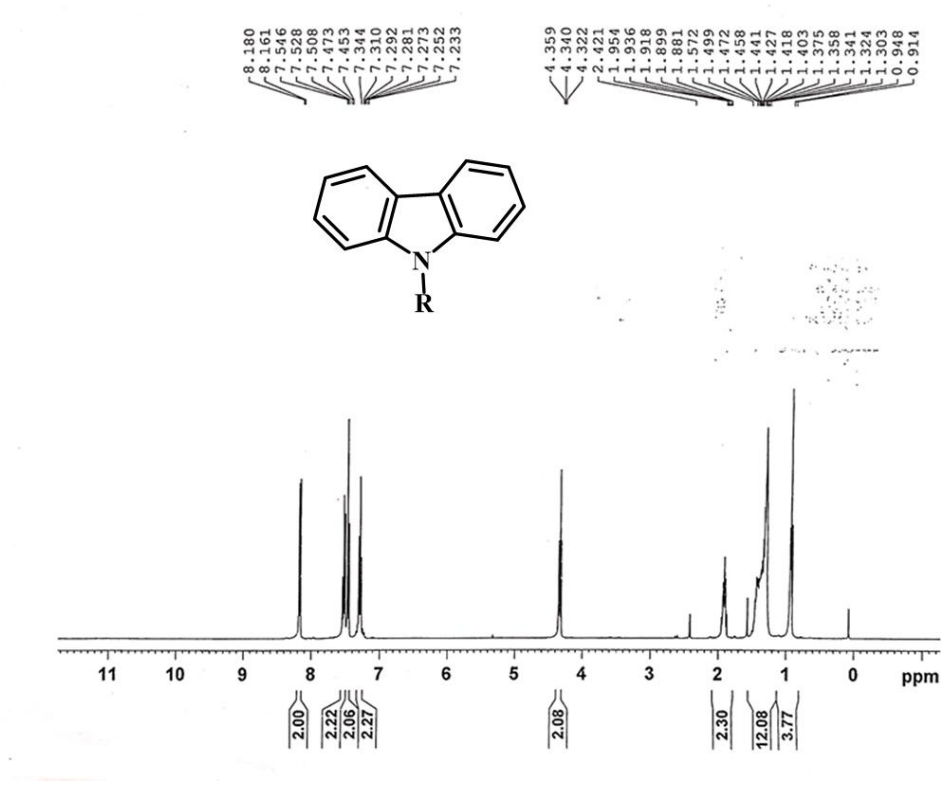

Figure 4.13 ^{1}H NMR spectra of **compound 1**

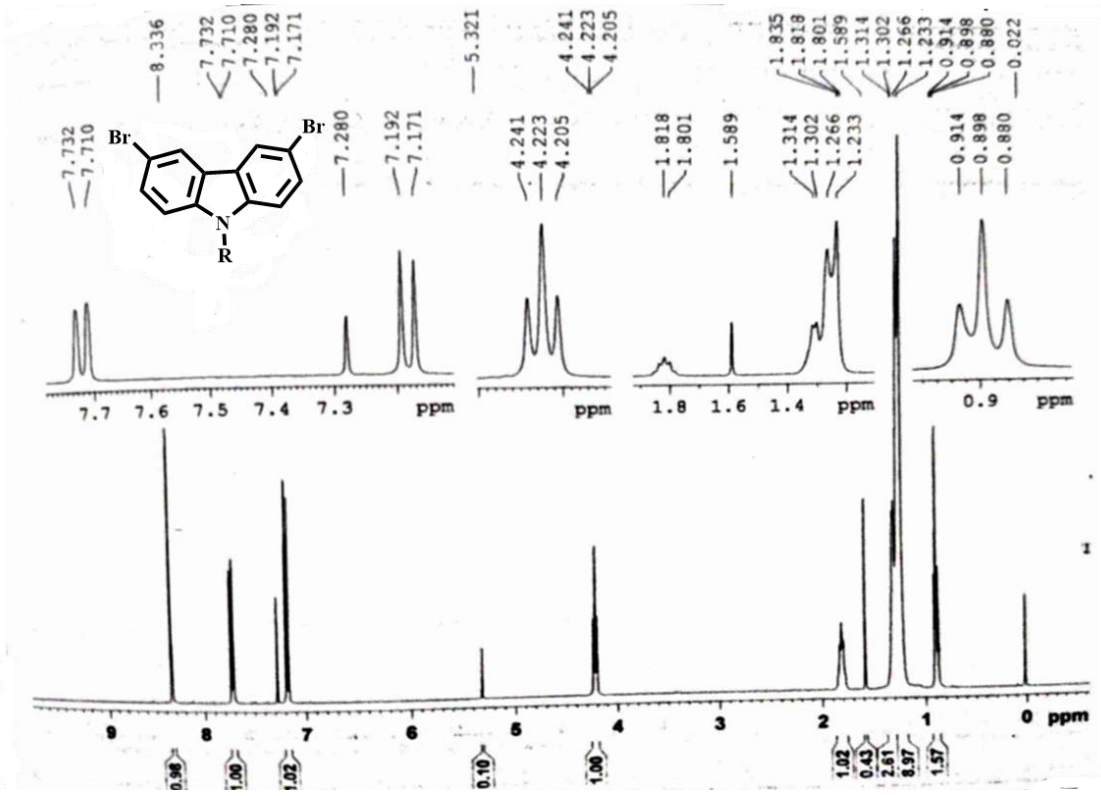

Figure 4.14 ^{1}H NMR spectra of **compound 2**

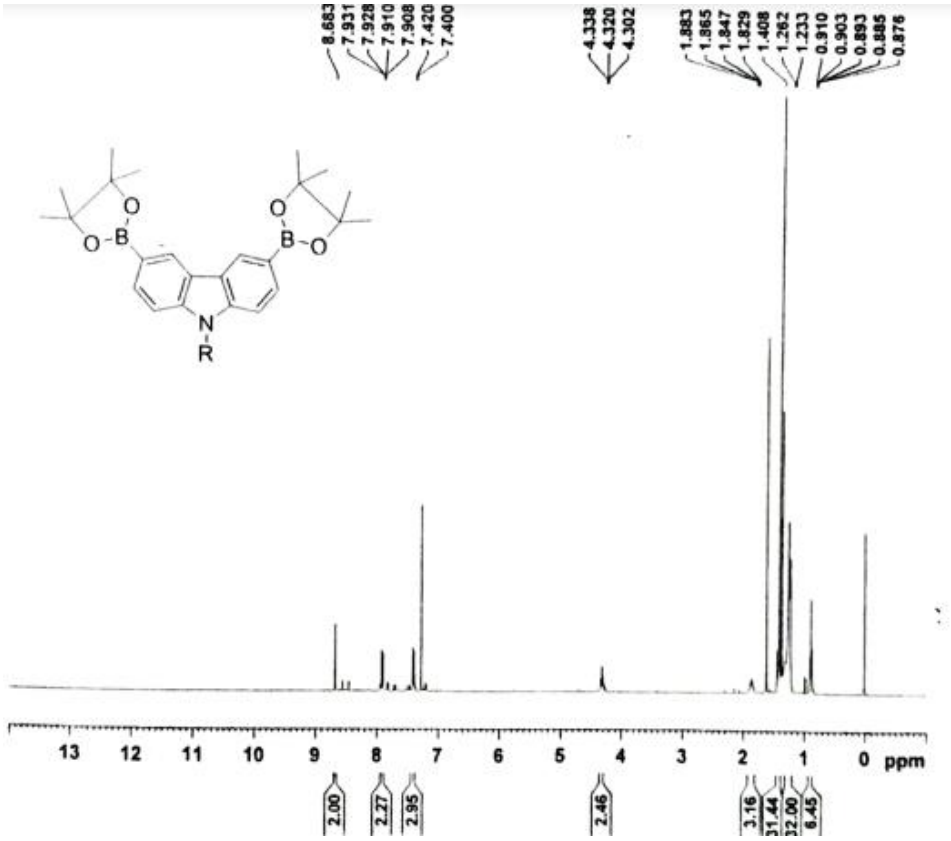

Figure 4.15 ^{1}H NMR spectra of **compound 3**

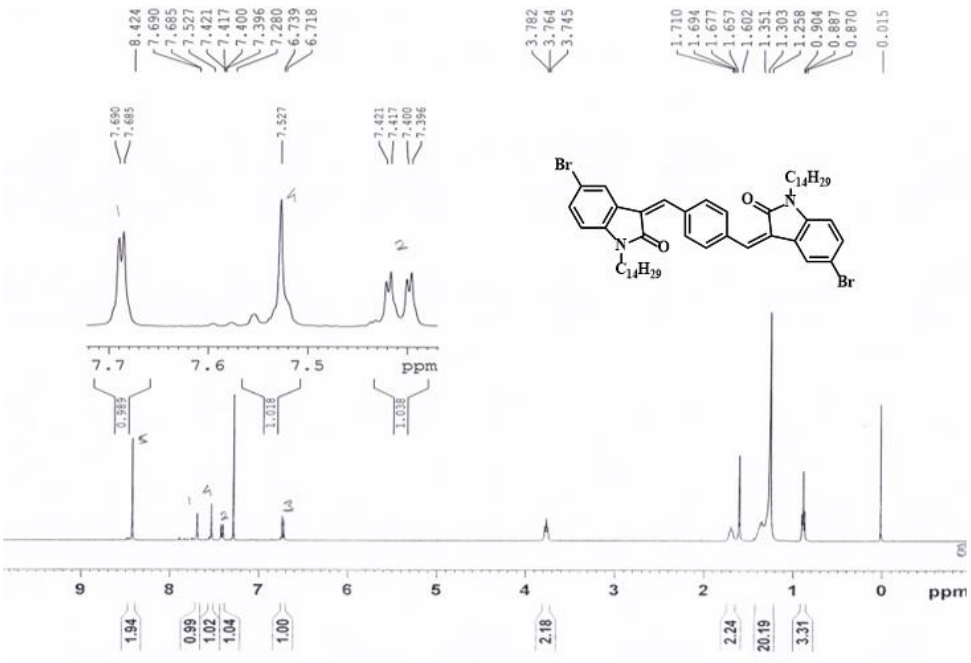

Figure 4.16 ^{1}H NMR spectra of **M1**

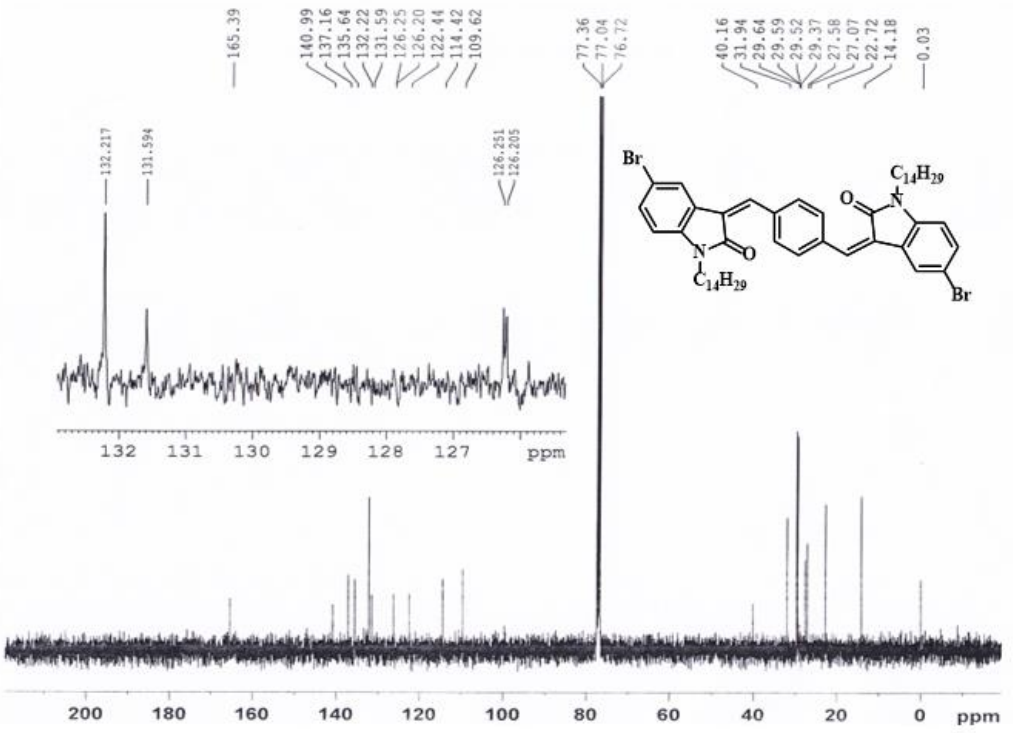

Figure 4.17 ^{13}C NMR spectra of **M1**

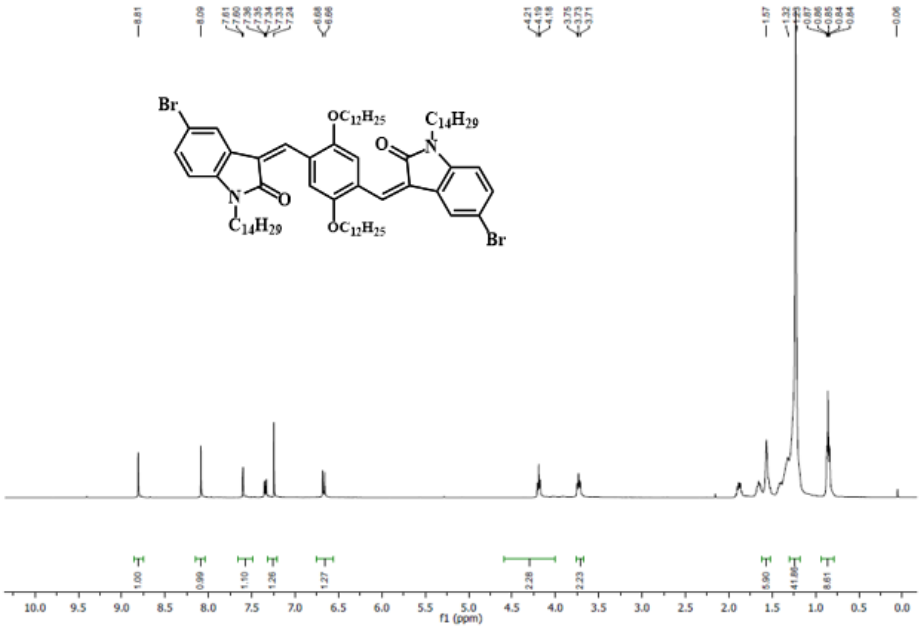

Figure 4.18 ^{1}H NMR spectra of **M2**

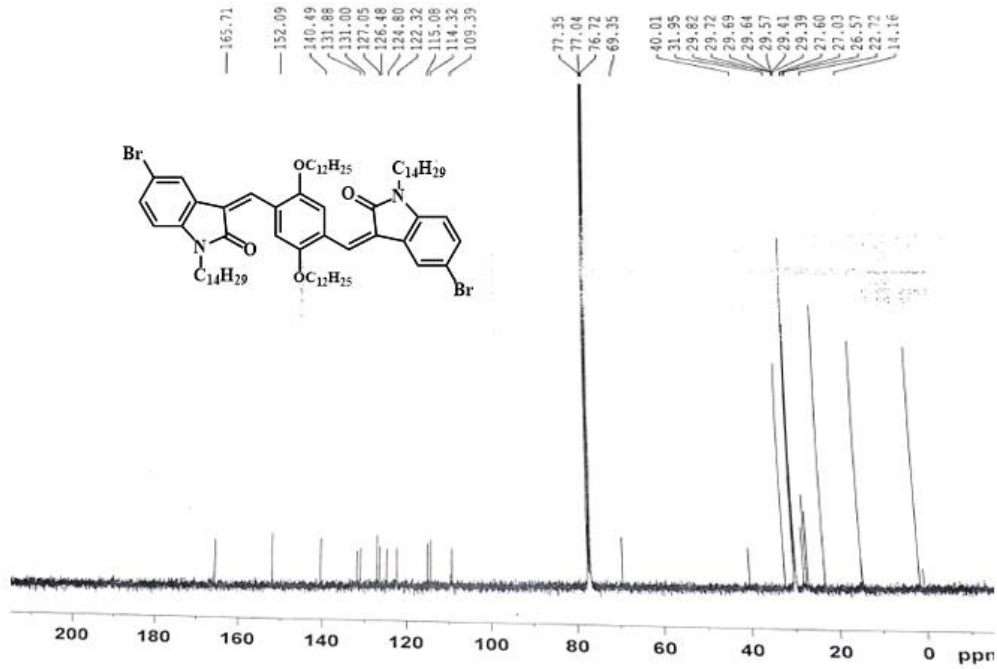

Figure 4.19 ^{13}C NMR spectra of **M2**

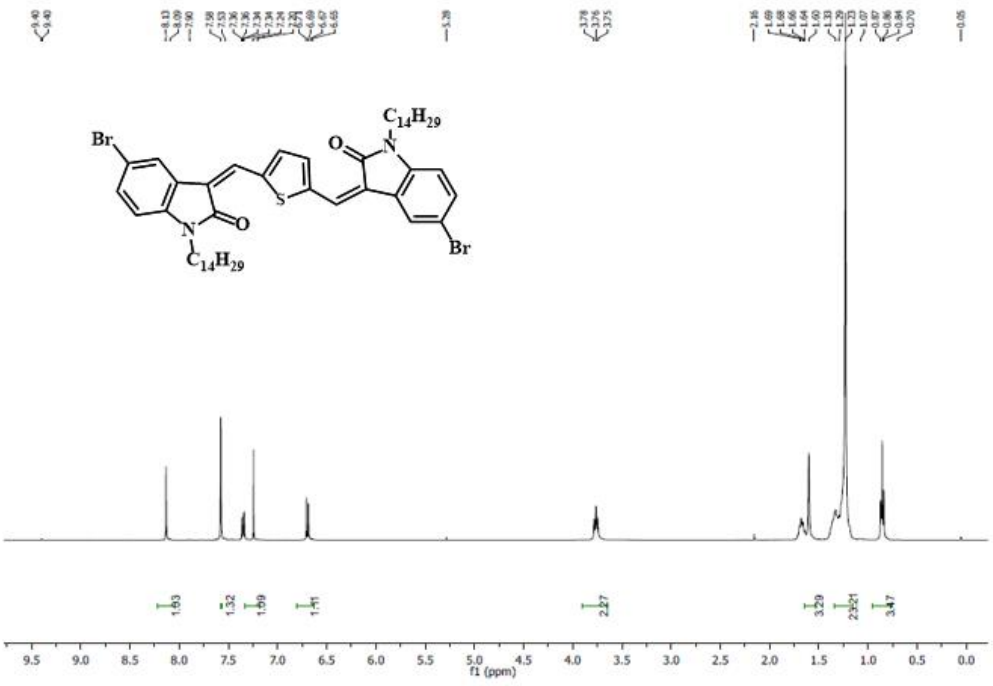

Figure 4.20 ^{1}H NMR spectra of **M3**

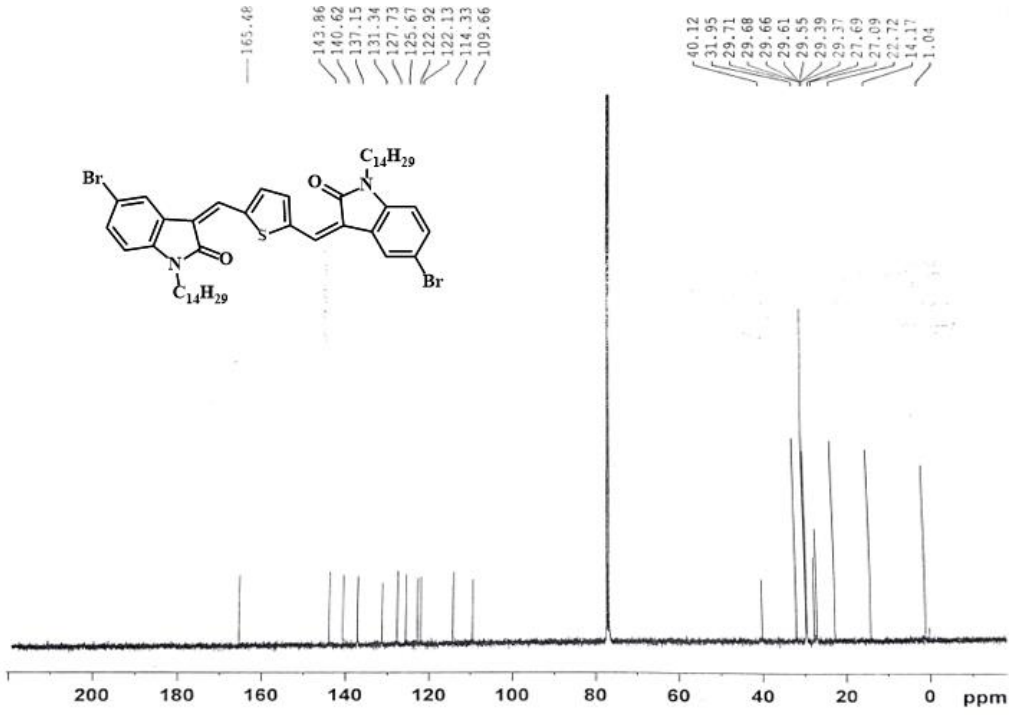

Figure 4.21 ^{13}C NMR spectra of **M3**

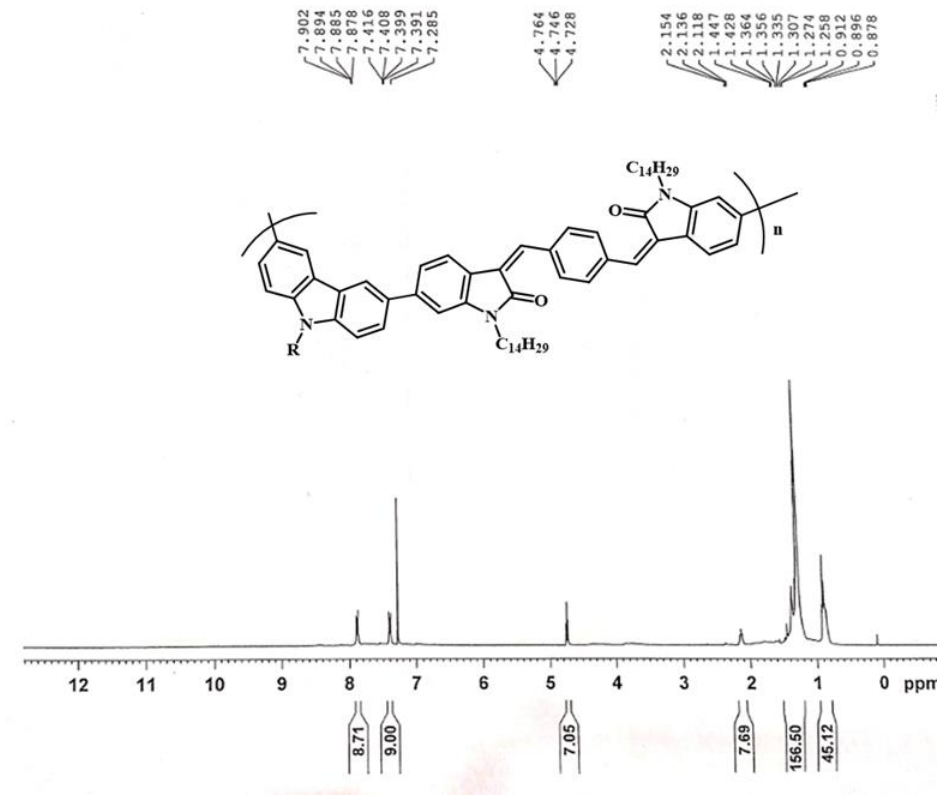

Figure 4.22 ^{1}H NMR spectra of **TIIG-BP**

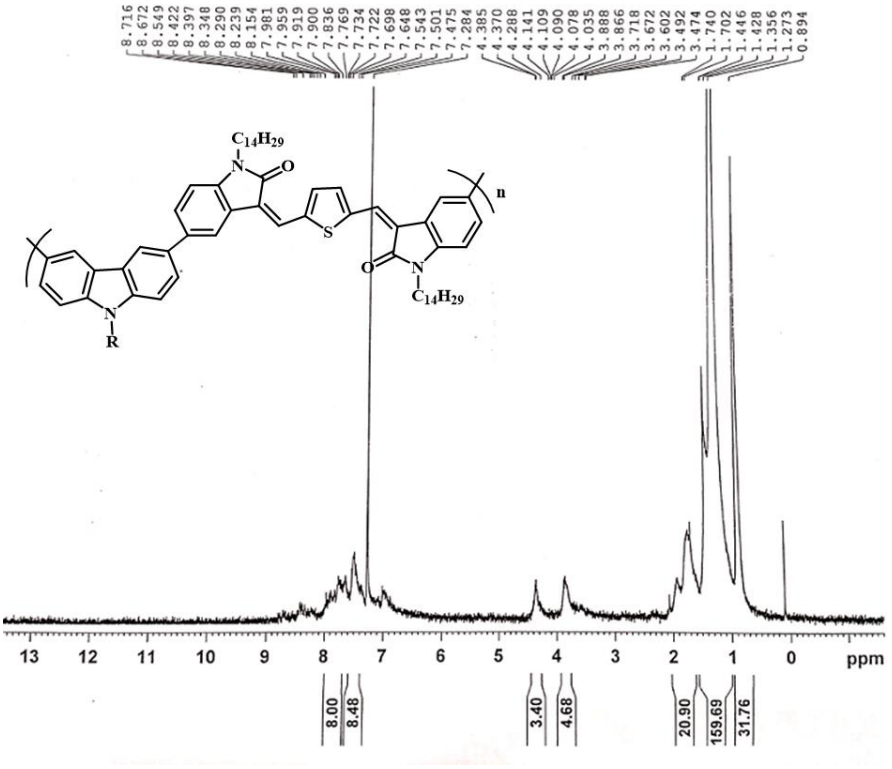

Figure 4.23 ^{1}H NMR spectra of **THP-BP**

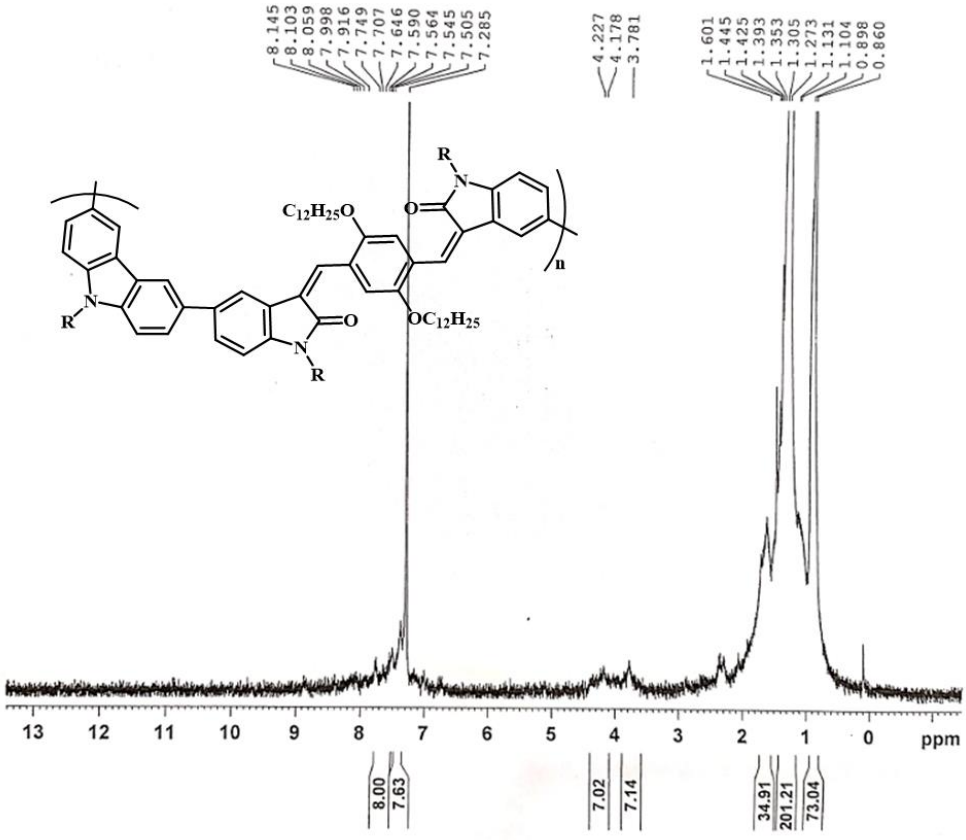

Figure 4.24 ^{1}H NMR spectra of **DAB-BP**

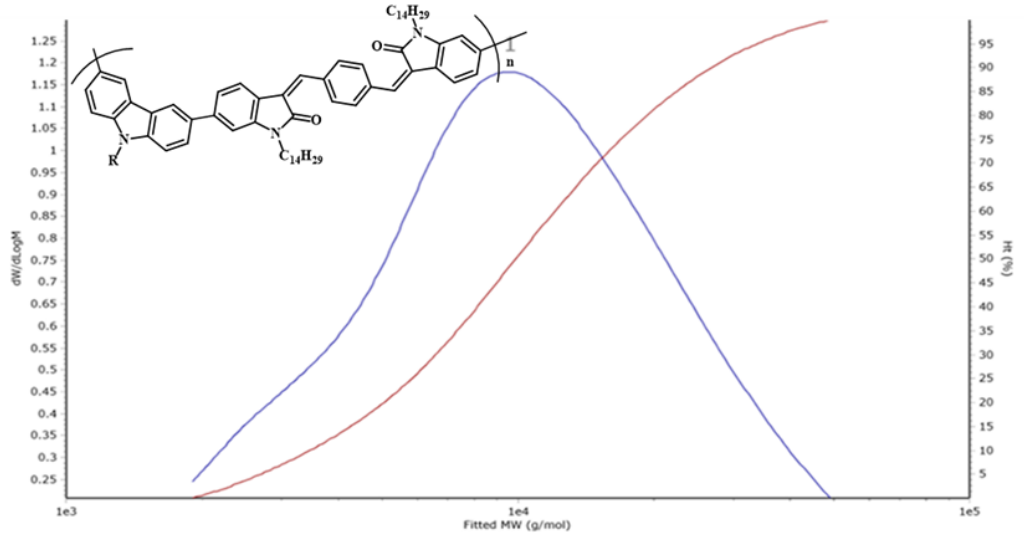

Results

Analysed by

Comments

Molecular Weight Averages

Peak	Mp (g/mol)	Mn (g/mol)	Mw (g/mol)	Mz (g/mol)	Mz+1 (g/mol)	Mv (g/mol)	PD
Peak 1	9788	7458	12827	20095	27033	19037	1.72

Figure 4.25 GPC analysis report of **TIIG-BP**

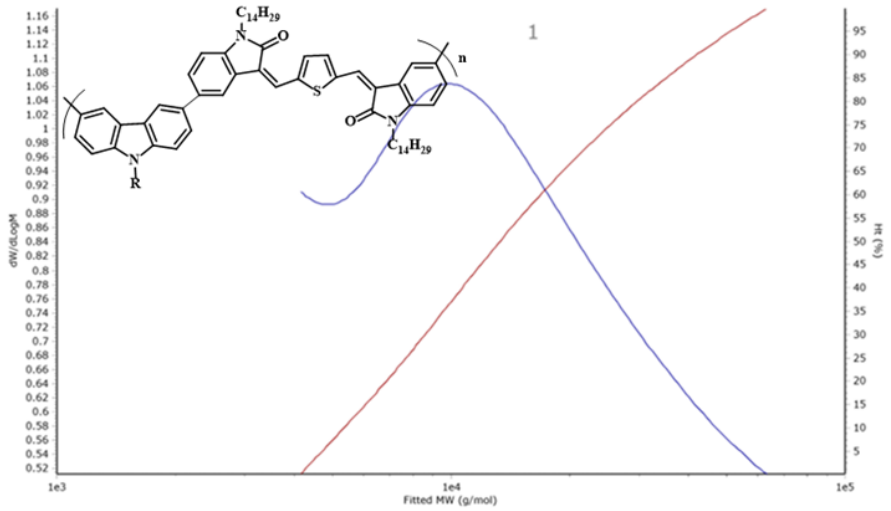

Results

Analysed by

Comments

Molecular Weight Averages

Peak	Mp (g/mol)	Mn (g/mol)	Mw (g/mol)	Mz (g/mol)	Mz+1 (g/mol)	Mv (g/mol)	PD
Peak 1	10265	11058	18703	29931	39631	28352	1.691

Figure 4.26 GPC analysis report of **THP-BP**

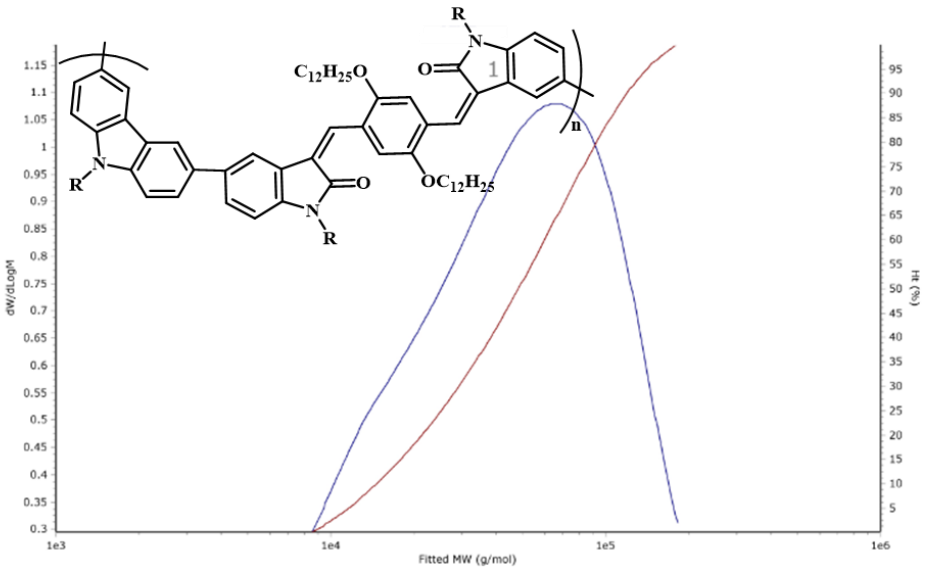

Results

Analysed by

Comments

Molecular Weight Averages

Peak	Mp (g/mol)	Mn (g/mol)	Mw (g/mol)	Mz (g/mol)	Mz+1 (g/mol)	Mv (g/mol)	PD
Peak 1	67260	33313	18480	86698	108724	83084	1.755

Figure 4.27 GPC analysis report of **DAB-BP**

References

1 M. Jahanfar, K. Tsuchiya and K. Ogino, *J. Photopolym. Sci. Technol.*, 2012, **25**, 333–334.

2 N. Blouin, A. Michaud and M. Leclerc, *Adv. Mater.*, 2007, **19**, 2295–2300.

3 N. Blouin and M. Leclerc, *Acc. Chem. Res*, 2008, **41**, 1–10.

4 J. Bouchard, S. Wakim and M. Leclerc, *J. Org. Chem.*, 2004, **69**, 5705–5711.

5 X. T. Tao, Y. D. Zhang, T. Wada, H. Sasabe, H. Suzuki, T. Watanabe and S. Miyata, *Adv. Mater.*, 1998, **10**, 226–230.

6 Z. B. Zhang, M. Fujiki, H. Z. Tang, M. Motonaga and K. Torimitsu, *Macromolecules*, 2002, **35**, 1988–1990.

7 P. T. B. Nicolas and B. Mario, 2008, 99–124.

8 Y. Takihana, M. Shiotsuki, F. Sanda and T. Masuda, *Macromolecules*, 2004, **37**, 7578–7583.

9 G. S. Liou, S. H. Hsiao and H. W. Chen, *J. Mater. Chem.*, 2006, **16**, 1831–1842.

10 N. Leclerc, A. Michaud, K. Sirois, J. F. Morin and M. Leclerc, *Adv. Funct. Mater.*, 2006, **16**, 1694–1704.

11 Z. B. Zhang, M. Motonaga, M. Fujiki and C. E. McKenna, *Macromolecules*, 2003, **36**, 6956–6958.

12 T. Michinobu, H. Kumazawa and K. Shigehara, *Chem. Lett.*, 2007, **36**, 620–621.

13 T. Michinobu, K. Okoshi, H. Osako, H. Kumazawa and K. Shigehara, *Polymer (Guildf).*, 2008, **49**, 192–199.

14 T. Michinobu, H. Osako and K. Shigehara, *Polymers (Basel).*, 2010, **2**, 159–173.

15 J. F. Morin and M. Leclerc, *Macromolecules*, 2001, **34**, 4680–4682.

16 S. H. Park, A. Roy, S. Beaupré, S. Cho, N. Coates, J. S. Moon, D. Moses, M. Leclerc, K. Lee and A. J. Heeger, *Nat. Photonics*, 2009, **3**, 297–303.

17 Y. Zou, D. Gendron, A. Najari, Y. Tao and M. Leclerc, 2009, 2891–2894.

18 D. Witker and J. R. Reynolds, *Macromolecules*, 2005, **38**, 7636–7644.

19 G. Zotti, G. Schiavon, S. Zecchin, J. F. Morin and M. Leclerc, *Macromolecules*, 2002, **35**, 2122–2128.

20 P. O. Morin, T. Bura and M. Leclerc, *Mater. Horizons*, 2016, **3**, 11–20.

21 J. V. Grazulevicius, P. Strohriegl, J. Pielichowski and K. Pielichowski, *Prog. Polym. Sci.*, 2003, **28**, 1297–1353.

22 S. H. Hsiao and S. W. Lin, *Polym. Chem.*, 2016, **7**, 198–211.

23 L. Jiaoli and G. Andrew C, *Chem. Soc. Rev.*, 2010, **39**, 2352–2353.

24 M. Nakamura, K. Yamabuki, T. Oishi and K. Onimura, *Polym. J.*, 2014, **46**, 94–103.

25 Y. S. Su and T. Y. Wu, *Polymers (Basel).*,polymers, 2017, **9(7)**, 284-302.

26 F. Bekkar, F. Bettahar, I. Moreno, R. Meghabar, M. Hamadouche, E. Hernáez, J. L. Vilas-Vilela and L. Ruiz-Rubio, *Polymers (Basel).*, 2020, **12**, 1–33.

27 D. Gerard, L.B. Lave, *Technological Forecasting & Social Change*, 2005, **27**761–778.

28 Y. Patil, R. Misra, M. L. Keshtov and G. D. Sharma, *J. Mater. Chem. A*, 2017, **5**, 3311–3319.

29 Y. Patil, T. Jadhav, B. Dhokale and R. Misra, *European J. Org. Chem.*, 2016, **2016**, 733–738.

30 K. Tani, N. Sakumoto, K. Kubono, K. Hori, Y. Tohda, H. Benten, H. Ohkita, S. Ito and M. Yamamoto, *Chem. Lett.*, 2009, **38**, 140–141.

31 O. K. Kwon, J. H. Park, D. W. Kim, S. K. Park and S. Y. Park, *Adv. Mater.*, 2015, **27**, 1951–1956.

32 Y. Lin, Q. He, F. Zhao, L. Huo, J. Mai, X. Lu, C. J. Su, T. Li, J. Wang, J. Zhu, Y. Sun, C. Wang and X. Zhan, *J. Am. Chem. Soc.*, 2016, **138**, 2973–2976.

33 R. Misra, T. Jadhav, B. Dhokale, P. Gautam, R. Sharma, R. Maragani and S. M. Mobin, *Dalt. Trans.*, 2014, **43**, 13076–13086.

34 K. Gao, L. Li, T. Lai, L. Xiao, Y. Huang, F. Huang, J. Peng, Y. Cao, F. Liu, T. P. Russell, R. A. J. Janssen and X. Peng, *J. Am. Chem. Soc.*, 2015, **137**, 7282–

7285.

35 V. Cimrová, D. Výprachtický, A. Růžička and V. Pokorná, *Polymers (Basel).*, 2023, **15(13)**, 2932-2953.

36 O. Kwon, J. Jo, B. Walker, G. C. Bazan and J. H. Seo, *J. Mater. Chem. A*, 2013, **1**, 7118–7124.

37 W. L. Gong, F. Zhong, M. P. Aldred, Q. Fu, T. Chen, D. K. Huang, Y. Shen, X. F. Qiao, D. Ma and M. Q. Zhu, *RSC Adv.*, 2012, **2**, 10821–10828.

38 G. Sathiyan, R. Thangamuthu and P. Sakthivel, *RSC Adv.*, 2016, **6**, 69196–69205.

39 E. V Dalessandro, H. P. Collin, L. G. L. Guimarães, M. S. Valle and J. R. J. Pliego, *J. Phys. Chem. B*, 2017, **121**, 5300–5307.

40 X. Zhao, L. Qian, J. Cao, S. Yan and L. Ding, *Polym. Chem.*, 2016, **7**, 1226–1229.

41 V. S. Kadam, P. A. Bhatt, H. K. Machhi, S. S. Soni, S. S. Zade and A. L. Patel, *Nano Sel.*, 2020, **1**, 491–498.

42 V. S. Kadam, H. K. Machhi, S. S. Soni, S. S. Zade and A. L. Patel, *New J. Chem.*, 2022, **46**, 8601-8610.

43 K. K. Sonigara, Z. Shao, J. Prasad, H. K. Machhi, G. Cui, S. Pang and S. S. Soni, *Adv. Funct. Mater.*, 2020, **30**, 1–9.

44 Y. Deng, B. Sun, Y. He, J. Quinn, C. Guo and Y. Li, *Angew. Chemie - Int. Ed.*, 2016, **55**, 3459–3462.